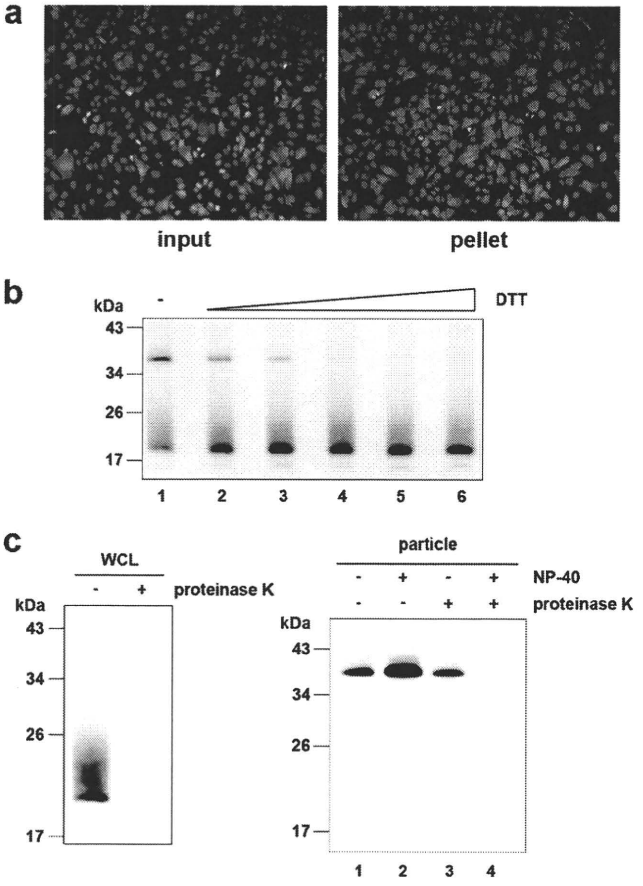

FIG. 1. The HCV-like particle consists of a core complex formed by a disulfide bond. (a) The infectivity of the pellet fraction collected from concentrated culture medium from JFH1^{E2FL} RNA-transfected HuH-7 cells was analyzed as described in Materials and Methods. Input indicates the same volume of concentrated culture medium used to pellet the virus-like particles. (b) Immunoblot analysis of the core protein in pellets containing JFH1^{E2FL} virus particles treated with various levels of DTT (lanes 1, 2, 3, 4, 5, and 6, 0, 1.56, 3.13, 6.25, 12.5, and 25 mM DTT, respectively). (c) Immunoblot analysis of the core protein in JFH1^{E2FL} particles collected from sucrose density gradient fractions with high HCV RNA titers (particle) (Fig. 2a, fractions 8 to 13) and treated with 5 μg/ml proteinase K at 37°C for 15 min in the presence or absence of 1% NP-40 (right panel). As a positive control, WCL prepared from JFH1^{E2FL} RNA-transfected HuH-7 cells in lysis buffer was treated with 5 μg/ml proteinase K at 37°C for 15 min (left panel). Data are representative of three independent experiments.

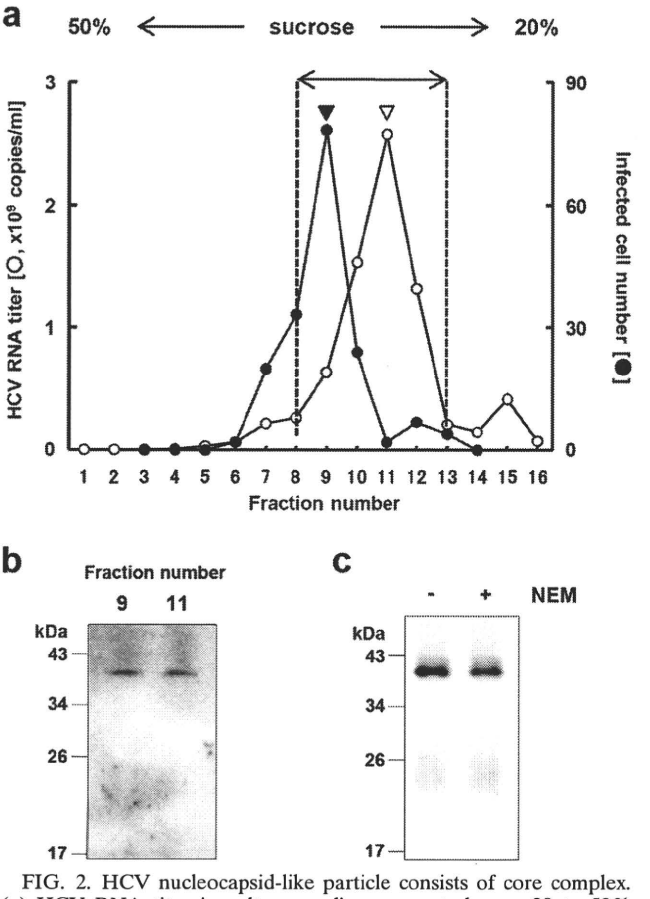

FIG. 2. HCV nucleocapsid-like particle consists of core complex. (a) HCV RNA titer in culture medium separated on a 20 to 50% sucrose density gradient. Concentrated culture medium from JFH1^{E2FL} RNA-transfected HuH-7 cells were treated with RNase and separated on a 20 to 50% sucrose density gradient. Fractions 1 to 16 were obtained from the bottom to the top of the tube, respectively. The HCV RNA titer and infectivity of each fraction were analyzed by real-time qRT-PCR (for fractions 1 to 16) and counting the number of cells infected with HCV-like particle detected by immunofluorescence (for fractions 3 to 14), respectively, as described in Materials and Methods. In brief, each fraction was diluted with 1× PBS and HCV-like particles were collected by ultracentrifugation, and then the pellets were suspended in culture medium and used for infection. (b) HCV-like particle collected from the infectious HCV peak (from panel a, filled arrowhead) and the HCV RNA peak (from panel a, open arrowhead) were collected by ultracentrifugation, subjected to nonreducing SDS-PAGE, and detected by immunoblotting against the core protein. (c) HCV-like particles collected from fractions 8 to 13 (a) were subjected to nonreducing SDS-PAGE in the presence (lane +) or absence (lane −) of 5 mM NEM and analyzed by immunoblotting against the core protein. Data are representative of two (a, infectivity of fractions) or three independent experiments.

PAGE under nonreducing conditions and showed only the dbc-complex (Fig. 1c, right panel).

To examine whether the complex contributes to the infectivity of the particles, we analyzed the dbc-complex in the fractions containing infectious and noninfectious HCV particles (fractions 9 and 11 of Fig. 2a, filled and open arrowheads, respectively). Both the infectious and noninfectious HCV particle-containing fractions contained the dbc-complex (Fig. 2b). To confirm this further, a pellet containing particles of mutant JFH1^{AAA99}—a mutant of JFH1^{E2FL} that primarily produces noninfectious particles (36)—was analyzed in a similar manner. These dbc-complexes were found in pelleted particles of both JFH1^{AAA99} and J6/JFH1^{AAA99}, which was a mutant J6/JFH1 with a similar substitution to JFH1^{AAA99} (see Fig. S2 in the supplemental material). These results indicated that the dbc-complex was present in both the infectious and noninfectious HCV-like particles.

The core protein monomer observed in the pellet samples (Fig. 1b) may be from the secreted core protein or the debris of apoptotic cells, because the core protein is known to be secreted from cells expressing this protein under particular conditions (42) and strain JFH1 is known to cause apoptosis (45). The dbc-complex-specific signals in the HCV particles seem to be increased in the NP-40-treated samples for some

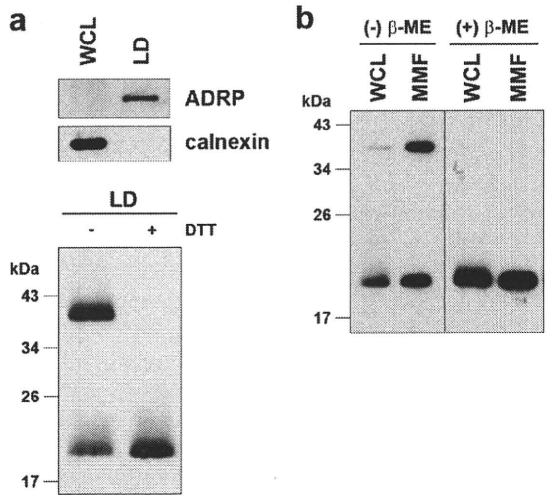

FIG. 3. The core complex is formed at the LD and ER. (a) The LD fraction and WCL were collected from JFH1^{E2FL} RNA-transfected HuH-7 cells on day 5 posttransfection. (upper panel) Immunoblot analysis of the LD marker ADRP and the ER marker calnexin in the LD fraction; (lower panel) immunoblot analysis of the core protein in the LD fraction treated or not treated with 50 mM DTT. (b) Immunoblot analysis of the core protein in the MMF and WCL collected from JFH1^{E2FL}-producing HuH-7 cells on day 5 posttransfection in the presence or absence of 5% β-ME. Data are representative of those from three independent experiments.

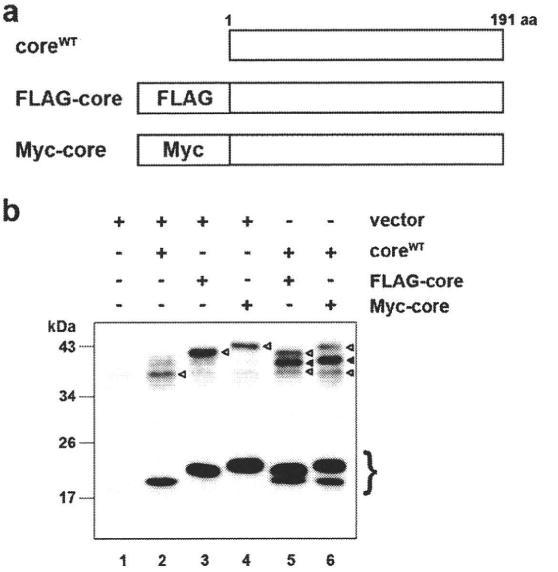

FIG. 4. The core complex consists of a core dimer. (a) Schematic of wild-type, FLAG-tagged (FLAG-core), and Myc-tagged (Myc-core) core proteins. (b) Immunoblot analysis of the core protein in the MMF collected from HuH-7 cells transfected with combinations of pcDNA3 (vector) and/or core expression plasmids (e.g., encoding core^{WT}, FLAG-core, and Myc-core), as indicated. The experiment was performed under nonreducing conditions. The lower bands represent core monomer (marked on the right with a brace). White arrowheads, bands corresponding to dbd-core; black arrowheads, positions of the intermediately sized core complex formed by core^{WT} and the tagged core. Data are representative of those from three independent experiments.

unknown reason (Fig. 1c, lanes 1 and 2). Although the intermolecular disulfide bond is known to be artificially formed in denaturing SDS-PAGE in the absence of reducing agents, the dbc-complex was still observed even in the presence of NEM, which is the alkylating agent for free sulfhydryls, during sample preparation (Fig. 2c), indicating that the dbc-complex was naturally present in the virus-like particles.

The HCV nucleocapsid is covered with lipid membranes and E1 and E2 proteins, making it resistant to proteases. As expected, in the absence of NP-40, the dbc-complex was resistant to proteinase K (Fig. 1c, lane 3), whereas proteinase K was able to digest core protein in whole-cell lysates (WCLs) collected from JFH1^{E2FL}-transfected HuH-7 cells (Fig. 1c, left panel). Disrupting the envelope structure with NP-40 made the dbc-complex susceptible to proteinase K treatment (Fig. 1c, lane 4), indicating that the dbc-complex was indeed a component of the HCV particle.

The dbc-complex forms on the ER. To investigate the subcellular site at which the dbc-complex forms, LDs and MMFs from JFH1^{E2FL} replicating HuH-7 cells were analyzed by immunoblotting. We first analyzed the dbc-complex in LDs, because LDs are involved in infectious HCV particle formation (36, 47). The purity of the LD fraction was determined using immunoblot analysis of calnexin and ADRP, ER and LD marker proteins, respectively (Fig. 3a, upper panel). The core protein was then analyzed in the LD fraction. As shown in Fig. 3a (lower panel), the dbc-complex was observed in the LD fraction from JFH1^{E2FL} RNA-transfected HuH-7 cells. We next analyzed the core protein in the ER-containing MMF, because the core protein is first translated and processed on the ER (16). As shown in Fig. 3b, the dbc-complex was observed in the MMF from JFH1^{E2FL} RNA-transfected HuH-7 cells. These results suggest that the dbc-complex is first formed at the ER. To assess the possibility that dbc-complex-containing HCV particles were also assembled on the ER, the sensitivity of the dbc-complex to protease treatment was analyzed. The dbc-complex in the MMF was susceptible to protease treatment in the absence of NP-40, indicating that the dbc-complex on the ER was not yet part of a HCV particle (data not shown).

dbc-complex is most likely a disulfide-bonded dimer form of the core. In order to examine whether the core protein itself has the potential to form a dbc-complex, we analyzed the dbc-complex formation of the full-length wild-type core protein (core^{WT}) expressed from pcDNA3-core^{WT} (36), the expression plasmid encoding the 191-amino-acid full-length core protein of JFH1 strain. We used this expression plasmid because the core protein from this plasmid was likely to be processed correctly enough to produce infectious HCV particles when it was cotransfected with the RNA of JFH1^{dc3}, which is a core protein deletion mutant of JFH1 (36). As a result, the dbc-complex formation was observed from the MMF of core^{WT}-expressing cells both in the absence and in the presence of NEM (Fig. 4b; lane 2 and data not shown, respectively). We next investigated the effect of the amino acid region of E1 on the production of the dbc-complex, because it has been reported that the efficient processing of core protein is dependent on the presence of some E1 sequence to ensure the insertion of the signal sequence for E1 in the translocon/membrane machinery (34). The dbc-complex was also observed

when the core protein was expressed from pcDNA3-C-E1/25, which encodes the full-length core protein followed by the N-terminal 25-amino-acid sequence of E1 to ensure that the core protein is processed properly (see Fig. S3a in the supplemental material). These data showed that the dbc-complex was formed by expression of the core protein only in the cells.

Next, we examined the structural components of the dbc-complex. Because the dbc-complex was twice the size of the core protein monomer, it was likely dbd-core. So, we investigated whether the core protein molecules with different tags were able to form the dbd-core. We first generated expression plasmids encoding core protein with the N-terminal FLAG and Myc tags (pcDNA3-FLAG-core and pcDNA3-Myc-core, respectively; Fig. 4a). The tagged core proteins were expressed or coexpressed with core^{WT} in HuH-7 cells, and the MMF was analyzed by immunoblotting. The FLAG or Myc tag shifted the positions of the monomer and the complex bands (Fig. 4b, lanes 3 and 4) compared with the position of core^{WT} (Fig. 4b, lane 2). When core^{WT} was coexpressed with FLAG-core or Myc-core, the core protein complex of an intermediate size was observed, in addition to the bands obtained when the constructs were independently expressed (Fig. 4b, lanes 5 and 6, filled arrowheads); the intermediate-sized band disappeared after treatment with β-ME (see Fig. S3b, lanes 11 and 12, filled arrows, in the supplemental material), indicating that core^{WT} and tagged core protein formed a heteromeric disulfide-bonded dimer. These results demonstrated that the dbc-complex on the ER is a dbd-core. Although we tried to detect the hetero- or homodimer consisting of the tagged core protein by using anti-FLAG or anti-Myc antibodies, these dimers were not detected, possibly because of the lower levels of sensitivity and specificity of the antibodies compared to those of the anti-core protein antibody that we used, especially against epitopes in the dbd-core. The results presented above, coupled with the similarities of the molecular sizes and sensitivities to β-ME and DTT, suggested that the dbc-complex in the HCV particle is most likely a dbd-core.

Core protein Cys128 mediates dbd-core formation. Our results showed that core protein from JFH1^{E2FL} forms a disulfide-bonded dimer on the ER. A search for cysteine residues in the JFH1^{E2FL} core protein identified amino acid positions 128 (Cys128) and 184 (Cys184) (see Fig. S1 in the supplemental material). These residues are highly conserved in core proteins from the approximately 2,000 reported HCV strains (HCVdb, http://www.hcvdb.org/, Hepatitis C Virus Database; http://s2as02.genes.nig.ac.jp/). To determine which cysteine residue mediated disulfide bond formation, we generated point mutations in JFH1^{E2FL} that replaced Cys128 and/or Cys184 with alanine (Ala) (C128A, C184A, and C128/184A in JFH1^{C128A}, JFH1^{C184A}, and JFH1$^{C128/184A}$, respectively; Fig. 5a). As shown in Fig. 5b, the core proteins from JFH1^{C128A} and JFH1$^{C128/184A}$ failed to form a dbd-core under nonreducing condition, whereas the core protein from JFH1^{C184A} formed the dimer, indicating that Cys128 was the residue responsible. Similar results were observed when Cys was replaced by serine (Ser) instead of Ala (see Fig. S5c in the supplemental material). Recently, Majeau et al. reported that the core protein of the J6/JFH1 strain with Cys128 replacements by Ala or Ser were unstable in both *Pichia pastoris* and human hepatoma cell line HuH-7.5 (31), although we did not detect any noticeable degradation of the mutant core proteins of strain JFH1 (Fig. 5b; see also Fig. S5c in the supplemental material). This difference may have resulted from the difference in sample preparation methods, as we used the full-length genome of JFH1^{E2FL} strain bearing the strain JFH1 core protein and HuH-7 cells instead of a core protein-expressing plasmid for the J6 strain and HuH-7.5 cells.

To exclude the possibility that mutation of Cys128 inhibited dbd-core formation by creating a conformational change, T127A and G129A core protein mutants (JFH1^{T127A} and JHF1^{G129A}, respectively) were created and examined for their effects on dbd-core formation and infectious virus particle production. These mutants formed dbd-core, and infectious HCV particles were detected in the culture medium (see Fig. S4a to c in the supplemental material), supporting an essential role for Cys128 in dbd-core and particle formation.

dbd-core contributes to HCV particle production. To examine the functional roles of dbd-core, infectious HCV particle production, HCV replication efficiency, colocalization of the core protein and LDs, and RNA binding of mutant and wild-type (JFH1^{E2FL}) core protein were evaluated. Culture medium from HuH-7 cells transfected with JFH1^{C128A} or JFH1$^{C128/184A}$ RNA contained significantly fewer infectious HCV particles compared with the numbers obtained with JFH1^{E2FL} or JFH1^{C184A} RNA (Fig. 5c). We also found significant decreases in the levels of HCV RNA and core protein in the culture medium of HuH-7 cells transfected with JFH1^{C128A} or JFH1$^{C128/184A}$ RNA (Fig. 5d and e). Similar results were observed with J6/JFH1 C128A or the C128/184A mutant strain (data not shown). To investigate whether these results were due to suppressed HCV replication, the HCV RNA and protein levels in cells transfected with mutant RNA were analyzed using qRT-PCR and immunoblot analyses, respectively. Compared with the results obtained with JFH1^{E2FL}, no significant changes in the cellular HCV RNA titer at days 1, 3, and 5 posttransfection or in the expression of HCV nonstructural protein NS5A were observed (Fig. 6a and b). This indicated that substitution of Cys128 did not significantly affect HCV RNA genome replication or viral protein production, demonstrating that the dbd-core functions during HCV particle production rather than HCV genome replication. Similar results were observed using RNA of JFH1 mutant strain JFH1^{C128S}, in which the cysteine at position 128 was replaced by Ser instead of Ala (see Fig. S5a, b, and d in the supplemental material).

The subcellular localizations of the core protein and NS5A protein in HuH-7 cells transfected with HCV RNA were investigated using indirect immunofluorescence and confocal microscopy, because recruiting HCV proteins to LDs is an important step in infectious HCV particle production (36, 47) and core trafficking to LDs is dependent on signal peptide peptidase (SPP)-mediated cleavage of the tail region (34, 41). JFH1^{C128A} mutant core protein and NS5A protein were efficiently trafficked to LDs, as was observed with wild-type JHF1^{E2FL} (Fig. 6c), suggesting that SPP cleavage and core protein maturation were not affected by the C128A mutation. Similar results were obtained with the core proteins derived from JFH1^{C184A} and JFH1$^{C128/184A}$ (see Fig. S6 in the supplemental material) and also Ser mutant JFH1^{C128S} (see Fig. 5e in the supplemental material).

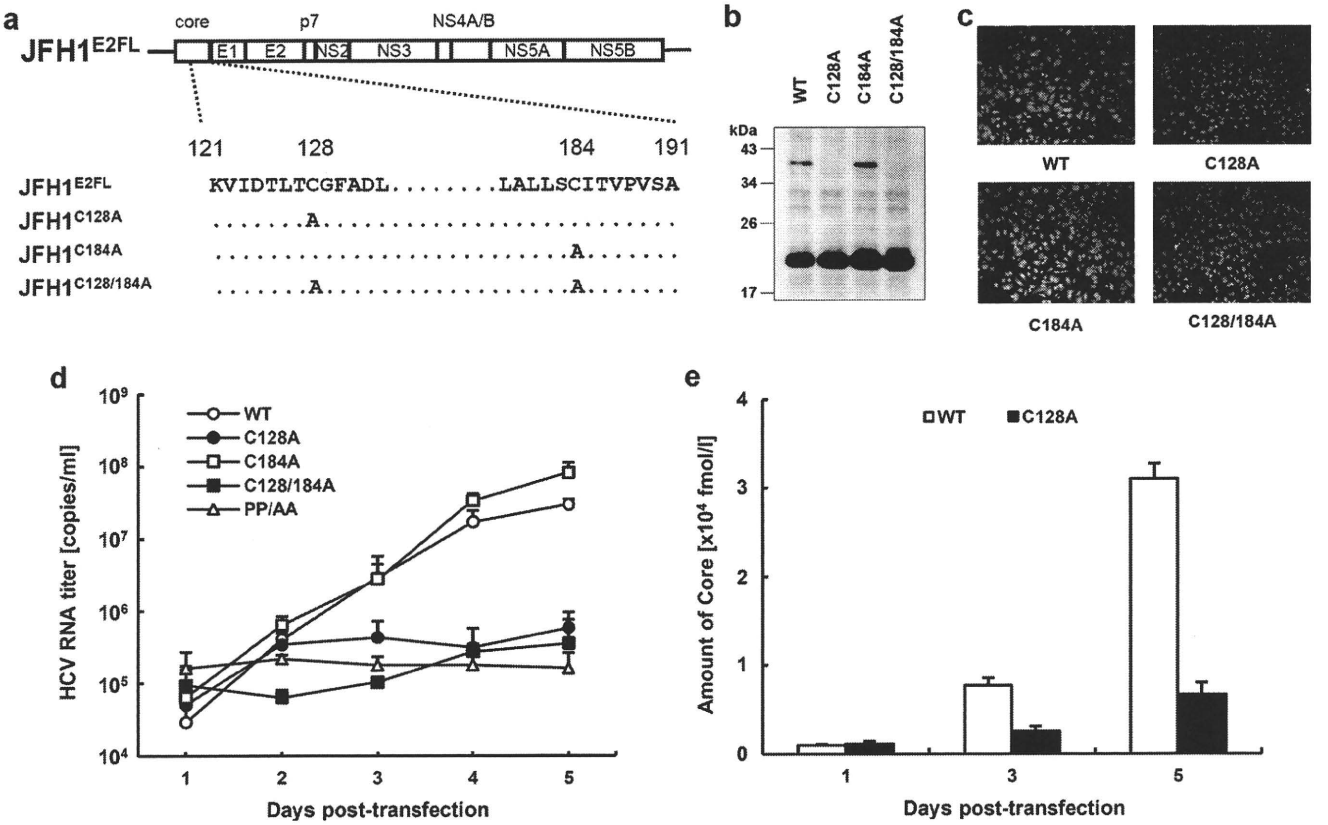

FIG. 5. The core dimer is formed via a bond between cysteine residues at amino acid position 128. (a) Site-directed mutagenesis of JFH1^{E2FL}. (b) Immunoblot analysis of the core protein in MMFs collected from HuH-7 cells under nonreducing conditions 3 days post-transfection with JFH1^{E2FL} (WT), JFH1^{C128A} (C128A), JFH1^{C184A} (C184A), or JFH1$^{C128/184A}$ (C128/184A) RNA. (c) Infectivity of culture medium collected and concentrated on day 5 posttransfection from HuH-7 cells transfected with WT, C128A, C184A, or C128/184A RNA. (d) Real-time qRT-PCR analysis of HCV RNA titers in culture medium collected at the indicated time points from HuH-7 cells transfected with WT, C128A, C184A, C128/184A, or PP/AA (JFH1$^{PP/AA}$) RNA. (e) ELISAs of core protein levels in culture medium collected at the indicated time points from HuH-7 cells transfected with WT or C128A RNA. Data are representative of those from three independent experiments (b and c) or are the means ± standard deviations from three independent experiments (d and e).

Because HCV core protein can bind to RNA, including the HCV genome, during viral particle assembly (43), we analyzed RNA binding by the core protein using *in vitro*-translated core^{C128A}, core^{WT}, and poly(U) agarose resin. Core^{C128A} and core^{WT} bound similarly to the poly(U) resin (Fig. 6d).

dbd-core is important for HCV particle assembly. The mutational analysis of the core protein indicated that core^{C128A} and core^{WT} similarly localize to LDs, recruit NS proteins to the LD, and bind to RNA. Moreover, this mutation did not markedly affect HCV genome replication. How does core^{C128A} affect the production of HCV particles? An important function of the core protein is multimerization, which is followed by capsid construction and packaging of the RNA genome in the viral particles. We therefore determined whether core^{C128A} had a dominant negative effect on virus-like particle production. Wild-type JFH1^{E2FL} RNA and different amounts of JFH1^{C128A} RNA were cotransfected into HuH-7 cells, and the HCV RNA titer and infectivity of the virus-like particles in the culture medium were analyzed. As expected, the HCV RNA titer in the cells increased with higher levels of transfected RNA (see Fig. S7a in the supplemental material). In contrast, the HCV RNA titer and infectivity in the culture medium decreased in a JFH1^{C128A} RNA dose-dependent manner when this mutant RNA was cotransfected with wild-type RNA (Fig. 7a, b). This suppressive effect was not observed when either wild-type RNA or core deletion mutant JFH1^{dc3} RNA was used instead of mutant RNA in a similar experiment (see Fig. S7b to e in the supplemental material), indicating that higher levels of HCV RNA alone did not inhibit HCV particle production. Thus, core^{C128A} had a dominant negative effect on HCV particle production. Together, these results suggest that dbd-core is involved in the assembly of HCV particles.

The nucleocapsid-like particle of HCV was resistant to trypsin treatment. To further investigate the structure of the HCV nucleocapsid-like particle most likely formed by dbd-core, we examined the sensitivity of the particle to trypsin, which cleaves polypeptides at the C-terminal end of basic residues. Whereas trypsin digested the core protein in the whole-cell lysates (Fig. 8a, left panel), dbd-core from buoyant density-fractionated JFH1^{E2FL} particles was resistant to digestion, despite NP-40 treatment (Fig. 8a, right panel), although it was sensitive to proteinase K, which has a broad specificity (Fig. 1c). The N-terminal hydrophilic domain of the core protein (from residues 6 to 121) contains a number of trypsin cleavage sites (25 sites

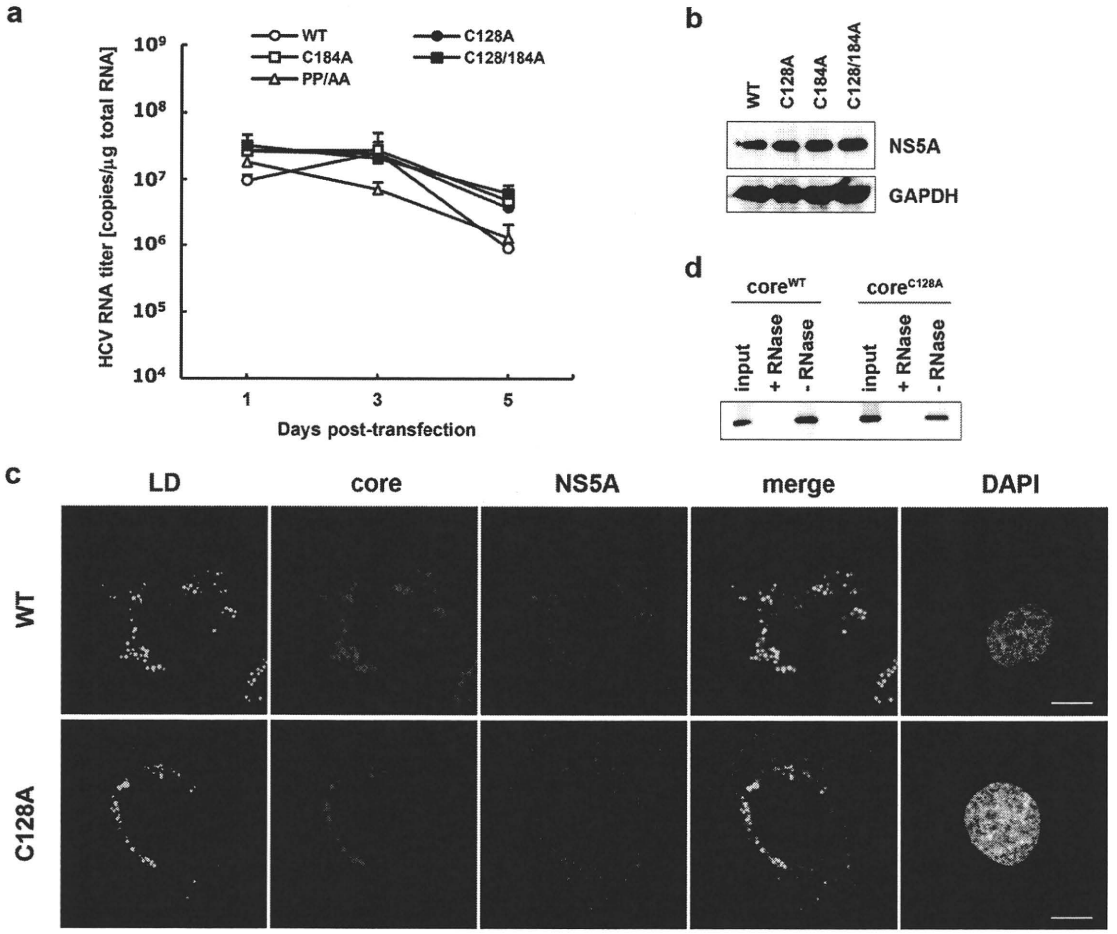

FIG. 6. Site-directed mutagenesis has no effect on HCV replication. (a) Real-time qRT-PCR analysis of the HCV RNA titer using total cellular RNA collected at the indicated time points from cells transfected with JFH1^{E2FL} (WT), JFH1^{C128A} (C128A), JFH1^{C184A} (C184A), JFH1$^{C128/184A}$ (C128/184A), or JFH1$^{PP/AA}$ (PP/AA) RNA. (b) Immunoblot analysis of NS5A protein and GAPDH in whole-cell lysate collected from cells transfected with WT, C128A, C184A, or C128/184A RNA at day 3 posttransfection. (c) Confocal microscopy of the subcellular localization of the LD (green), core (blue), NS5A protein (red), and nucleus (4′,6-diamidino-2-phenylindole [DAPI]) (gray) in WT and C128A replicating cells on day 3 posttransfection. Bars, 10 μm. (d) An RNA-protein binding precipitation assay was performed with *in vitro*-translated core^{WT} and core^{C128A} using poly(U) agarose as the resin. +RNase and −RNase, samples with and without RNase treatment, respectively, as described in Materials and Methods. Input indicates that 1/40 of the amount of translated product was used in this assay. Data represent the means ± standard deviations from three independent experiments (a) or are representative of those from three independent experiments (b to d).

in strain JHF1) (see Fig. S1 in the supplemental material), suggesting that the N-terminal domain faces inward and/or that the conformation prevents protease access. To address this idea, buoyant density-fractionated JFH1^{E2FL} particles were treated with trypsin under stricter conditions in the presence of NP-40. Cleavage of dbd-core by various levels of trypsin correlated with the appearance of a shorter molecule (Fig. 8b, white arrowhead). The shorter molecule was presumed to be partially digested dbd-core with an intact N-terminal region because it was recognized by anti-core protein antibodies, which bind to an epitope located from amino acids 20 to 40 of the core protein (M. Kohara, The Tokyo Metropolitan Institute of Medical Science, personal communication). These results suggest that dbd-core is assembled into the nucleocapsid-like particle such that most of the N-terminal domain is inside.

DISCUSSION

In the present study, we have shown that the nucleocapsid-like particle of HCV most likely contains a dimer of core protein that is stabilized by a disulfide bond. Mutational analysis revealed that Cys128 forms a disulfide bond between core monomers. Several reports have shown that disulfide bonds in the capsid proteins of some viruses are involved in virus particle assembly and stabilization of the viral capsid structure (4, 21, 27, 28, 57); these viruses are characterized by icosahedral nucleocapsids. Because, like these viruses, the HCV virion is spherical (2, 20), it has been suggested that HCV may contain a nucleocapsid with a similar structure (20). We found the dbc-complex, which is most likely to be the dbd-core in JFH1^{E2FL} virus-like particles (Fig. 1c and 8a). The dbd-core in the capsid structure was digested by proteinase K but not

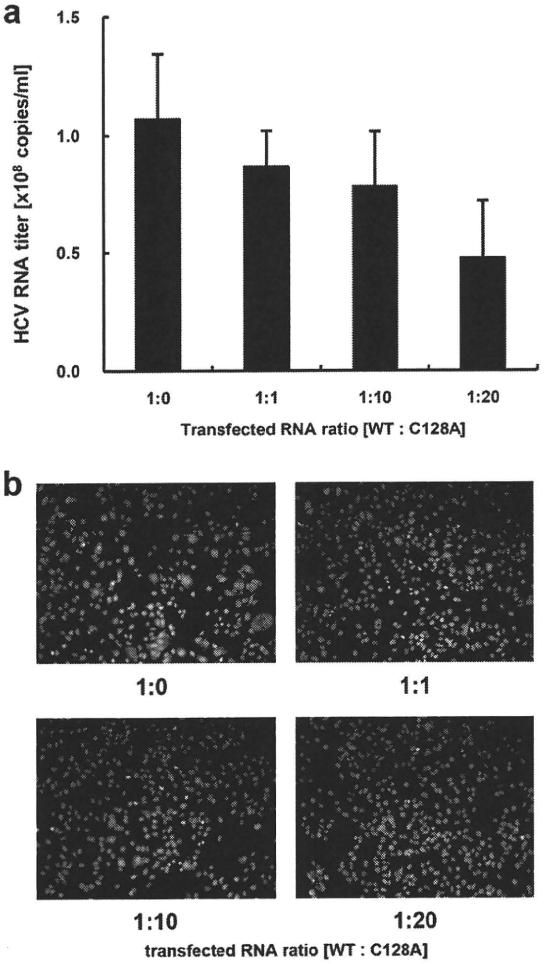

FIG. 7. JFH1^{C128A} core inhibits JFH1^{E2FL} particle assembly. A competitive inhibitory assay was performed with JFH1^{E2FL} (WT) and JFH1^{C128A} (C128A). (a) Real-time qRT-PCR analysis of the HCV RNA titer in HuH-7 cell culture medium 3 days after the cells were transfected with the indicated ratio of WT and C128A RNA. (b) The infectivity of culture medium collected from HuH-7 cells that had been transfected with the indicated ratio of WT and C128A RNA was analyzed as described in Materials and Methods. Data represent the means ± standard deviations from three independent experiments (a) or are representative of those from three independent experiments (b).

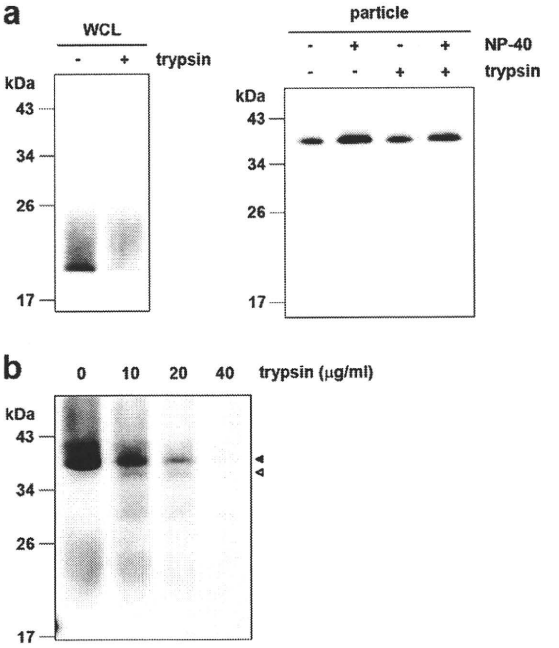

FIG. 8. The nucleocapsid-like particle of JFH1^{E2FL} is assembled with the C-terminal region of the core protein on the outer surface. (a) Immunoblot analysis of the core protein in JFH1^{E2FL} particles collected from sucrose density gradient fractions with high HCV RNA titers (particle) (Fig. 2a, fractions 8 to 13). The fractions were treated with 10 μg/ml trypsin at 37°C for 15 min in the presence or absence of 1% NP-40 (right panel). As a positive control, WCL prepared from JFH1^{E2FL} RNA-transfected HuH-7 cells in lysis buffer was treated with 10 μg/ml trypsin at 37°C for 15 min (left panel). (b) Immunoblot analysis of the core protein in JFH1^{E2FL} particles collected from sucrose density gradient fractions with high HCV RNA titers (Fig. 2a, fractions 8 to 13). The fractions were treated with the indicated concentrations of trypsin at 37°C for 10 min in the presence of 1% NP-40. Open and filled arrows indicate the positions of dbd-core and the trypsin-digested fragment, respectively. Data are representative of those from three independent experiments.

trypsin in the presence of NP-40 (Fig. 1c and 8a, lane 4). The resistance to trypsin suggested a tight conformation for dbd-core in the capsid and no exposed trypsin cleavage sites. The truncated form of dbd-core that was observed under certain trypsin treatment conditions likely resulted from cleavage in the C-terminal portion of the protein (e.g., arginine residues at positions 149 and 156) (see Fig. S1 in the supplemental material), although it is possible that the truncation of dbd-core was due to nonspecific cleavage by trypsin. These results imply that dbd-core is configured such that the N- and C-terminal ends are located at the inner and outer surfaces of the capsid, respectively. Because the N-terminal region of the core protein includes the RNA binding domain (43), the HCV RNA genome likely interacts with the core protein as it is packed in the nucleocapsid. On the other hand, the C-terminal hydrophobic domain probably faces the lipid membranes to form the envelope structure. Only part of the N-terminal hydrophilic region of the core protein has been structurally examined using X-ray crystal structural analysis (35) and structural bioinformatics and nuclear magnetic resonance analysis (11). Although the C-terminal half of the core protein has been structurally investigated by the use of bioinformatics (8), the three-dimensional structure containing the Cys128 residue is unknown. Thus, determination of the structure of the core protein in the nucleocapsid containing the Cys128 residue should be required for understanding the whole structure of this protein in the virus particles.

Because cotransfection of JFH1^{C128A} RNA with wild-type JFH1^{E2FL} RNA inhibited particle production in a mutant RNA dose-dependent manner (Fig. 7a and b), the C128A core variant clearly inhibited HCV particle formation by wild-type core protein. Cys128 was also previously reported to be a residue included in the region important for the production of infectious HCV (39). This residue is located near the N-terminal end of the hydrophobic region of the core (amino acids 122 to 177) and belongs to the hydrophilic side of an amphipathic helix expected to interact in the plane of the membrane interface (7). Therefore, it is possible to think that dbd-core

formation via Cys128 can stabilize the interaction between the core protein and the membranes. The N-terminal half of the core protein (amino acids 1 to 124) reportedly assembles into nucleocapsid-like particles in the presence of the 5′ UTR from HCV RNA (24), suggesting that some nucleocapsid-like particles may assemble via only homotypic interactions from the core protein. In addition to weak homotypic interactions, the HCV core protein forms a disulfide bond to stabilize the capsid structure, thus making dbd-core indispensable in the stable virus-like particle. We observed that culture medium from JFH1^{C128A}- or JFH1^{C128S}-transfected cells included slight infectivity (Fig. 5c; see also Fig. S5d in the supplemental material). This made us speculate that this mutant may produce some infective particle-like structure formed by a homotypic interaction of the core. Such a slight infectivity may have reflected the optimized *in vitro* culture conditions compared with the *in vivo* conditions, allowing relatively unstable virus particles to survive.

A nucleocapsid must be resistant to environmental degradation yet still be able to disassemble after infection. Disulfide bonds could help with this process by switching between a stable and unstable virus capsid on the basis of different intracellular and extracellular oxidation conditions (12, 30). During the virus life cycle, the disulfide bond strengthens the viral capsid structure and protects the viral genome from oxidative conditions and cellular nucleases when virus particles are formed. Upon infection, the disulfide bond may be cleaved under cytoplasmic reducing conditions, thereby releasing the viral genome into the cell for replication. HCV may utilize the core protein disulfide bond in this way as HCV enters the host cell via clathrin-mediated endocytosis (5) into a low-pH, endosomal compartment (25, 52); this is presumably followed by endosomal membrane fusion and release of the viral capsid into the cytoplasm (38).

Treatment of HCV infection with pegylated interferon in combination with ribavirin is not effective for all patients. Recently, drugs targeting viral proteins NS3/4A and NS5B have been examined in clinical trials. Although these drugs are relatively specific, resulting in fewer side effects and potent antiviral activity, monotherapy can be complicated by rapidly emerging resistant variants carrying mutations that reduce drug efficacy, perhaps due to conformational changes in the target (23, 48, 51). Therefore, viral proteins that are highly conserved among strains and those characterized by low mutation rates may be better targets for drug development. Because the core protein is the most conserved HCV protein and Cys128 is conserved among almost all HCV strains examined, drugs that interact with Cys128 and/or the region around or near this residue will likely show broad-spectrum efficacy to block stable infectious particle formation. Structural analysis of dbd-core should aid with the development of new STAT-Cs that target Cys128 by direct interaction with the sulfide group and/or region around this residue. Until now and still, the mechanism of disulfide bond formation of the core protein on the ER is unknown. Dimerization of the capsid protein by disulfide bond has been reported in some enveloped viruses (9, 19, 54, 56), although some were shown not to be important for virus particle formation (26, 55). Unlike vaccinia virus (46), no redox system of its own has been reported for these viruses. Therefore, further investigations addressing the mechanisms underlying dbd-core formation on the ER may reveal a new mechanism for disulfide bond formation of viral proteins in infected cells.

ACKNOWLEDGMENTS

This work was supported by grants-in-aid from the Ministry of Health, Labor, and Welfare of Japan and by grants-in-aid from the Japan Health Sciences Foundation.

REFERENCES

1. **Abid, K., V. Pazienza, A. de Gottardi, L. Rubbia-Brandt, B. Conne, P. Pugnale, C. Rossi, A. Mangia, and F. Negro.** 2005. An in vitro model of hepatitis C virus genotype 3a-associated triglycerides accumulation. J. Hepatol. **42:**744–751.
2. **Aly, H. H., Y. Qi, K. Atsuzawa, N. Usuda, Y. Takada, M. Mizokami, K. Shimotohno, and M. Hijikata.** 2009. Strain-dependent viral dynamics and virus-cell interactions in a novel in vitro system supporting the life cycle of blood-borne hepatitis C virus. Hepatology **50:**689–696.
3. **Asselah, T., Y. Benhamou, and P. Marcellin.** 2009. Protease and polymerase inhibitors for the treatment of hepatitis C. Liver Int. **29**(Suppl. 1):57–67.
4. **Baron, M. D., and K. Forsell.** 1991. Oligomerization of the structural proteins of rubella virus. Virology **185:**811–819.
5. **Blanchard, E., S. Belouzard, L. Goueslain, T. Wakita, J. Dubuisson, C. Wychowski, and Y. Rouille.** 2006. Hepatitis C virus entry depends on clathrin-mediated endocytosis. J. Virol. **80:**6964–6972.
6. **Boulant, S., M. W. Douglas, L. Moody, A. Budkowska, P. Targett-Adams, and J. McLauchlan.** 2008. Hepatitis C virus core protein induces lipid droplet redistribution in a microtubule- and dynein-dependent manner. Traffic **9:**1268–1282.
7. **Boulant, S., R. Montserret, R. G. Hope, M. Ratinier, P. Targett-Adams, J. P. Lavergne, F. Penin, and J. McLauchlan.** 2006. Structural determinants that target the hepatitis C virus core protein to lipid droplets. J. Biol. Chem. **281:**22236–22247.
8. **Boulant, S., C. Vanbelle, C. Ebel, F. Penin, and J. P. Lavergne.** 2005. Hepatitis C virus core protein is a dimeric alpha-helical protein exhibiting membrane protein features. J. Virol. **79:**11353–11365.
9. **Cornillez-Ty, C. T., and D. W. Lazinski.** 2003. Determination of the multimerization state of the hepatitis delta virus antigens in vivo. J. Virol. **77:**10314–10326.
10. **Dustin, L. B., and C. M. Rice.** 2007. Flying under the radar: the immunobiology of hepatitis C. Annu. Rev. Immunol. **25:**71–99.
11. **Duvignaud, J. B., C. Savard, R. Fromentin, N. Majeau, D. Leclerc, and S. M. Gagne.** 2009. Structure and dynamics of the N-terminal half of hepatitis C virus core protein: an intrinsically unstructured protein. Biochem. Biophys. Res. Commun. **378:**27–31.
12. **Freedman, R. B., B. E. Brockway, and N. Lambert.** 1984. Protein disulphide-isomerase and the formation of native disulphide bonds. Biochem. Soc. Trans. **12:**929–932.
13. **Giannini, C., and C. Brechot.** 2003. Hepatitis C virus biology. Cell Death Differ. **10**(Suppl. 1):S27–S38.
14. **Grakoui, A., C. Wychowski, C. Lin, S. M. Feinstone, and C. M. Rice.** 1993. Expression and identification of hepatitis C virus polyprotein cleavage products. J. Virol. **67:**1385–1395.
15. **Higashi, Y., H. Itabe, H. Fukase, M. Mori, Y. Fujimoto, R. Sato, T. Imanaka, and T. Takano.** 2002. Distribution of microsomal triglyceride transfer protein within sub-endoplasmic reticulum regions in human hepatoma cells. Biochim. Biophys. Acta **1581:**127–136.
16. **Hijikata, M., N. Kato, Y. Ootsuyama, M. Nakagawa, and K. Shimotohno.** 1991. Gene mapping of the putative structural region of the hepatitis C virus genome by in vitro processing analysis. Proc. Natl. Acad. Sci. U. S. A. **88:**5547–5551.
17. **Hijikata, M., H. Mizushima, Y. Tanji, Y. Komoda, Y. Hirowatari, T. Akagi, N. Kato, K. Kimura, and K. Shimotohno.** 1993. Proteolytic processing and membrane association of putative nonstructural proteins of hepatitis C virus. Proc. Natl. Acad. Sci. U. S. A. **90:**10773–10777.
18. **Hope, R. G., and J. McLauchlan.** 2000. Sequence motifs required for lipid droplet association and protein stability are unique to the hepatitis C virus core protein. J. Gen. Virol. **81:**1913–1925.
19. **Hu, H. M., K. N. Shih, and S. J. Lo.** 1996. Disulfide bond formation of the in vitro-translated large antigen of hepatitis D virus. J. Virol. Methods **60:**39–46.
20. **Ishida, S., M. Kaito, M. Kohara, K. Tsukiyama-Kohora, N. Fujita, J. Ikoma, Y. Adachi, and S. Watanabe.** 2001. Hepatitis C virus core particle detected by immunoelectron microscopy and optical rotation technique. Hepatol. Res. **20:**335–347.
21. **Jeng, K. S., C. P. Hu, and C. M. Chang.** 1991. Differential formation of disulfide linkages in the core antigen of extracellular and intracellular hepatitis B virus core particles. J. Virol. **65:**3924–3927.
22. **Kato, N., M. Hijikata, Y. Ootsuyama, M. Nakagawa, S. Ohkoshi, T. Sug-**

imura, and K. Shimotohno. 1990. Molecular cloning of the human hepatitis C virus genome from Japanese patients with non-A, non-B hepatitis. Proc. Natl. Acad. Sci. U. S. A. **87:**9524–9528.
23. **Kieffer, T. L., A. D. Kwong, and G. R. Picchio.** 2010. Viral resistance to specifically targeted antiviral therapies for hepatitis C (STAT-Cs). J. Antimicrob. Chemother. **65:**202–212.
24. **Kim, M., Y. Ha, and H. J. Park.** 2006. Structural requirements for assembly and homotypic interactions of the hepatitis C virus core protein. Virus Res. **122:**137–143.
25. **Koutsoudakis, G., A. Kaul, E. Steinmann, S. Kallis, V. Lohmann, T. Pietschmann, and R. Bartenschlager.** 2006. Characterization of the early steps of hepatitis C virus infection by using luciferase reporter viruses. J. Virol. **80:**5308–5320.
26. **Lee, J. Y., D. Hwang, and S. Gillam.** 1996. Dimerization of rubella virus capsid protein is not required for virus particle formation. Virology **216:**223–227.
27. **Li, M., P. Beard, P. A. Estes, M. K. Lyon, and R. L. Garcea.** 1998. Intercapsomeric disulfide bonds in papillomavirus assembly and disassembly. J. Virol. **72:**2160–2167.
28. **Li, P. P., A. Nakanishi, S. W. Clark, and H. Kasamatsu.** 2002. Formation of transitory intrachain and interchain disulfide bonds accompanies the folding and oligomerization of simian virus 40 Vp1 in the cytoplasm. Proc. Natl. Acad. Sci. U. S. A. **99:**1353–1358.
29. **Liang, T. J., L. J. Jeffers, K. R. Reddy, M. De Medina, I. T. Parker, H. Cheinquer, V. Idrovo, A. Rabassa, and E. R. Schiff.** 1993. Viral pathogenesis of hepatocellular carcinoma in the United States. Hepatology **18:**1326–1333.
30. **Liljas, L.** 1999. Virus assembly. Curr. Opin. Struct. Biol. **9:**129–134.
31. **Majeau, N., R. Fromentin, C. Savard, M. Duval, M. J. Tremblay, and D. Leclerc.** 2009. Palmitoylation of hepatitis C virus core protein is important for virion production. J. Biol. Chem. **284:**33915–33925.
32. **Matsumoto, M., S. B. Hwang, K. S. Jeng, N. Zhu, and M. M. Lai.** 1996. Homotypic interaction and multimerization of hepatitis C virus core protein. Virology **218:**43–51.
33. **McLauchlan, J.** 2000. Properties of the hepatitis C virus core protein: a structural protein that modulates cellular processes. J. Viral Hepat. **7:**2–14.
34. **McLauchlan, J., M. K. Lemberg, G. Hope, and B. Martoglio.** 2002. Intramembrane proteolysis promotes trafficking of hepatitis C virus core protein to lipid droplets. EMBO J. **21:**3980–3988.
35. **Menez, R., M. Bossus, B. H. Muller, G. Sibai, P. Dalbon, F. Ducancel, C. Jolivet-Reynaud, and E. A. Stura.** 2003. Crystal structure of a hydrophobic immunodominant antigenic site on hepatitis C virus core protein complexed to monoclonal antibody 19D9D6. J. Immunol. **170:**1917–1924.
36. **Miyanari, Y., K. Atsuzawa, N. Usuda, K. Watashi, T. Hishiki, M. Zayas, R. Bartenschlager, T. Wakita, M. Hijikata, and K. Shimotohno.** 2007. The lipid droplet is an important organelle for hepatitis C virus production. Nat. Cell Biol. **9:**1089–1097.
37. **Moradpour, D., C. Englert, T. Wakita, and J. R. Wands.** 1996. Characterization of cell lines allowing tightly regulated expression of hepatitis C virus core protein. Virology **222:**51–63.
38. **Moradpour, D., F. Penin, and C. M. Rice.** 2007. Replication of hepatitis C virus. Nat. Rev. Microbiol. **5:**453–463.
39. **Murray, C. L., C. T. Jones, J. Tassello, and C. M. Rice.** 2007. Alanine scanning of the hepatitis C virus core protein reveals numerous residues essential for production of infectious virus. J. Virol. **81:**10220–10231.
40. **Nolandt, O., V. Kern, H. Muller, E. Pfaff, L. Theilmann, R. Welker, and H. G. Krausslich.** 1997. Analysis of hepatitis C virus core protein interaction domains. J. Gen. Virol. **78**(Pt 6):1331–1340.
41. **Okamoto, K., Y. Mori, Y. Komoda, T. Okamoto, M. Okochi, M. Takeda, T. Suzuki, K. Moriishi, and Y. Matsuura.** 2008. Intramembrane processing by signal peptide peptidase regulates the membrane localization of hepatitis C virus core protein and viral propagation. J. Virol. **82:**8349–8361.
42. **Sabile, A., G. Perlemuter, F. Bono, K. Kohara, F. Demaugre, M. Kohara, Y. Matsuura, T. Miyamura, C. Brechot, and G. Barba.** 1999. Hepatitis C virus core protein binds to apolipoprotein AII and its secretion is modulated by fibrates. Hepatology **30:**1064–1076.
43. **Santolini, E., G. Migliaccio, and N. La Monica.** 1994. Biosynthesis and biochemical properties of the hepatitis C virus core protein. J. Virol. **68:**3631–3641.
44. **Seeff, L. B., and J. H. Hoofnagle.** 2003. Appendix: The National Institutes of Health Consensus Development Conference Management of Hepatitis C 2002. Clin. Liver Dis. **7:**261–287.
45. **Sekine-Osajima, Y., N. Sakamoto, K. Mishima, M. Nakagawa, Y. Itsui, M. Tasaka, Y. Nishimura-Sakurai, C. H. Chen, T. Kanai, K. Tsuchiya, T. Wakita, N. Enomoto, and M. Watanabe.** 2008. Development of plaque assays for hepatitis C virus-JFH1 strain and isolation of mutants with enhanced cytopathogenicity and replication capacity. Virology **371:**71–85.
46. **Senkevich, T. G., C. L. White, E. V. Koonin, and B. Moss.** 2000. A viral member of the ERV1/ALR protein family participates in a cytoplasmic pathway of disulfide bond formation. Proc. Natl. Acad. Sci. U. S. A. **97:**12068–12073.
47. **Shavinskaya, A., S. Boulant, F. Penin, J. McLauchlan, and R. Bartenschlager.** 2007. The lipid droplet binding domain of hepatitis C virus core protein is a major determinant for efficient virus assembly. J. Biol. Chem. **282:**37158–37169.
48. **Shimakami, T., R. E. Lanford, and S. M. Lemon.** 2009. Hepatitis C: recent successes and continuing challenges in the development of improved treatment modalities. Curr. Opin. Pharmacol. **9:**537–544.
49. **Tellinghuisen, T. L., M. J. Evans, T. von Hahn, S. You, and C. M. Rice.** 2007. Studying hepatitis C virus: making the best of a bad virus. J. Virol. **81:**8853–8867.
50. **Tellinghuisen, T. L., and C. M. Rice.** 2002. Interaction between hepatitis C virus proteins and host cell factors. Curr. Opin. Microbiol. **5:**419–427.
51. **Thompson, A. J., and J. G. McHutchison.** 2009. Antiviral resistance and specifically targeted therapy for HCV (STAT-C). J. Viral Hepat. **16:**377–387.
52. **Tscherne, D. M., C. T. Jones, M. J. Evans, B. D. Lindenbach, J. A. McKeating, and C. M. Rice.** 2006. Time- and temperature-dependent activation of hepatitis C virus for low-pH-triggered entry. J. Virol. **80:**1734–1741.
53. **Wakita, T., T. Pietschmann, T. Kato, T. Date, M. Miyamoto, Z. Zhao, K. Murthy, A. Habermann, H. G. Krausslich, M. Mizokami, R. Bartenschlager, and T. J. Liang.** 2005. Production of infectious hepatitis C virus in tissue culture from a cloned viral genome. Nat. Med. **11:**791–796.
54. **Wootton, S. K., and D. Yoo.** 2003. Homo-oligomerization of the porcine reproductive and respiratory syndrome virus nucleocapsid protein and the role of disulfide linkages. J. Virol. **77:**4546–4557.
55. **Zhou, S., and D. N. Standring.** 1992. Cys residues of the hepatitis B virus capsid protein are not essential for the assembly of viral core particles but can influence their stability. J. Virol. **66:**5393–5398.
56. **Zhou, S., and D. N. Standring.** 1992. Hepatitis B virus capsid particles are assembled from core-protein dimer precursors. Proc. Natl. Acad. Sci. U. S. A. **89:**10046–10050.
57. **Zweig, M., C. J. Heilman, Jr., and B. Hampar.** 1979. Identification of disulfide-linked protein complexes in the nucleocapsids of herpes simplex virus type 2. Virology **94:**442–450.

Hepatitis C Virus Controls Interferon Production through PKR Activation

Noëlla Arnaud[1], Stéphanie Dabo[1], Patrick Maillard[1], Agata Budkowska[1], Katerina I. Kalliampakou[2], Penelope Mavromara[2], Dominique Garcin[3], Jacques Hugon[4], Anne Gatignol[5], Daisuke Akazawa[6], Takaji Wakita[6], Eliane F. Meurs[1]*

1 Institut Pasteur, Unité Hépacivirus et Immunité Innée, Paris, France, **2** Hellenic Pasteur Institute, Molecular Virology Laboratory, Athens, Greece, **3** University of Geneva School of Medicine, Geneva, Switzerland, **4** Institut du Fer à Moulin, Inserm UMRS 839, Paris, France, **5** Lady Davis Institute for Medical Research, Virus-Cell Interactions, McGill University, Montréal, Canada, **6** National Institute of Infectious Diseases, Department of Virology II, Tokyo, Japan

Abstract

Hepatitis C virus is a poor inducer of interferon (IFN), although its structured viral RNA can bind the RNA helicase RIG-I, and activate the IFN-induction pathway. Low IFN induction has been attributed to HCV NS3/4A protease-mediated cleavage of the mitochondria-adapter MAVS. Here, we have investigated the early events of IFN induction upon HCV infection, using the cell-cultured HCV JFH1 strain and the new HCV-permissive hepatoma-derived Huh7.25.CD81 cell subclone. These cells depend on ectopic expression of the RIG-I ubiquitinating enzyme TRIM25 to induce IFN through the RIG-I/MAVS pathway. We observed induction of IFN during the first 12 hrs of HCV infection, after which a decline occurred which was more abrupt at the protein than at the RNA level, revealing a novel HCV-mediated control of IFN induction at the level of translation. The cellular protein kinase PKR is an important regulator of translation, through the phosphorylation of its substrate the eIF2α initiation factor. A comparison of the expression of luciferase placed under the control of an eIF2α-dependent ($IRES^{EMCV}$) or independent ($IRES^{HCV}$) RNA showed a specific HCV-mediated inhibition of eIF2α-dependent translation. We demonstrated that HCV infection triggers the phosphorylation of both PKR and eIF2α at 12 and 15 hrs post-infection. PKR silencing, as well as treatment with PKR pharmacological inhibitors, restored IFN induction in JFH1-infected cells, at least until 18 hrs post-infection, at which time a decrease in IFN expression could be attributed to NS3/4A-mediated MAVS cleavage. Importantly, both PKR silencing and PKR inhibitors led to inhibition of HCV yields in cells that express functional RIG-I/MAVS. In conclusion, here we provide the first evidence that HCV uses PKR to restrain its ability to induce IFN through the RIG-I/MAVS pathway. This opens up new possibilities to assay PKR chemical inhibitors for their potential to boost innate immunity in HCV infection.

Citation: Arnaud N, Dabo S, Maillard P, Budkowska A, Kalliampakou KI, et al. (2010) Hepatitis C Virus Controls Interferon Production through PKR Activation. PLoS ONE 5(5): e10575. doi:10.1371/journal.pone.0010575

Editor: Sung Key Jang, Pohang University of Science and Technology, Republic of Korea

Received January 13, 2010; **Accepted** April 16, 2010; **Published** May 11, 2010

Funding: Financial support was provided by grants from Institut Pasteur (IP) and CNRS (URA3015). Noella Arnaud is recipient of Ministère de l'Education et de la Recherche fellowship. The funders had no role in study design, data collection and analysis, decision to publish, or preparation of the manuscript.

Competing Interests: The authors have declared that no competing interests exist.

* E-mail: emeurs@pasteur.fr

Introduction

In response to invasion with bacterial or viral pathogens, cells are able to mount an immediate immune response through their ability to use specialized cellular molecules, referred to as pattern recognition receptors or PRRs, to detect unusual DNA, ssRNA or dsRNA structures. Among these PRRs, are the CARD-containing DexD/H RNA helicases RIG-I and MDA5, which are activated upon binding either to both 5′-triphosphate ssRNA and short double-stranded RNA structures (RIG-I) or to long dsRNA and higher-ordered RNA structures (MDA5) [1]. Once activated, these RNA helicases interact with the mitochondria-bound MAVS adapter protein [2]. In the case of RIG-I, the interaction with MAVS requires ubiquitination of the CARD domain of RIG-I by the TRIM25 ubiquitin ligase [3]. Subsequently, MAVS is able to recruit the IKK complex and the TBK1/IKKε kinases that are responsible for the activation of the NF-κB and IRF3/IRF7 transcription factors, respectively. This leads to induction of the interferons and pro-inflammatory cytokines that are involved in the innate immune response [4].

Hepatitis C virus (HCV) (*Hepacivirus* genus within the *Flaviviridae* family) is one of the RIG-I-activating viruses [4], because of its 5′ppp-structured RNA, 3′-structured genomic RNA and replicative RNA duplexes [5]. In particular, its 3′-end poly-U/UC motif has been shown to function in conjunction with the 5′ppp as the HCV structure that activates RIG-I [6].

In contrast to other RIG-I activating viruses such as Sendai virus, influenza, or vesicular stomatitis virus [1], HCV is a poor inducer of IFN and pro-inflammatory cytokines in cell culture systems. One reason for this is that the HCV NS3/4A protease cleaves MAVS, resulting in a rapid disruption of the function of MAVS and in abrogation of the IFN induction pathway [2]. However, data presented in some studies performed using Huh7 hepatoma cells infected with cell-culture generated JFH1 virus showed that the IFN pathway was poorly activated even before full cleavage of MAVS, since only limited nuclear translocation of

IRF3 could be detected [7,8]. Similarly, in another study, infection of Huh7 cells with JFH1 did not lead to any IFN induction, whereas the cells responded well to transfection by synthetic dsRNA poly(I)-poly(C) [9]. Thus, the early events leading to IFN induction after RIG-I activation by HCV are still not well-characterized.

Here, we have re-addressed the question as to whether HCV infection can activate RIG-I/MAVS before cleavage of MAVS by the NS3/4A protease, by performing kinetics of infection with JFH1 in the newly described JFH1-permissive Huh7.25/CD81 cells, which were manipulated to present a functional RIG-I/MAVS pathway. Our results show that HCV infection can stimulate the IFN induction pathway up to 12 hrs post-infection, whereas detection of MAVS cleavage begins at 18 hrs post-infection and is maximal at 24 hrs. Importantly, our data reveal that 12 hrs post-infection, HCV promotes a rapid inhibition of IFN induction at the level of translation, indicating a new mechanism of regulation. We demonstrated that this regulation was linked to activation of the dsRNA-activated eIF2α kinase PKR [10]. Altogether, our results show that HCV uses PKR to control the translation of newly transcribed IFN mRNAs before sufficient NS3/4A protein can be synthesized to efficiently restrain transcription of IFN.

Results

Ectopic expression of TRIM25 allows IFN induction in JFH1 permissive Huh7.25/CD81 cells to be studied

There is at present no satisfactory cell culture system that is both permissive for HCV and presents an intact RIG-I pathway. For instance, the Huh7.5 cells, which were cloned from the hepatoma Huh7 cells for their efficacy to support HCV replication [11], are unable to stimulate IFN induction because of a T55I substitution in the first CARD domain of RIG-I that prevents the association of RIG-I with MAVS [5]. Recently, another Huh7 subclone that could efficiently replicate the JFH1 subgenomic replicon (clone Huh7.25) was stably transfected with the essential HCV CD81 receptor, to generate Huh7.25/CD81 cells that are highly permissive to infection by JFH1[12]. We compared the ability of Huh7.25/CD81, Huh7.5 and Huh7 cells to activate the IFN inducing pathway after transfection with an IFNβ-luciferase reporter and infection with Sendai virus (Figure 1). The results showed that Huh7.25/CD81 cells are defective in the IFN-inducing pathway, similarly to Huh7.5 cells. In contrast, Huh7 cells can mount a robust IFN induction in response to infection with Sendai virus. Interestingly, whereas ectopic expression of MAVS in both Huh7.25/CD81 and Huh7.5 cells resulted in a strong stimulation of IFNβ-luciferase, ectopic expression of RIG-I was not able to restore the IFN-inducing pathway in Huh7.25/CD81 cells, in contrast to in Huh7.5 cells where it was able to do so as expected. This indicated that the defect in Huh7.25/CD81 cells was upstream of MAVS and either at the level of RIG-I or downstream of RIG-I. Since efficient activation of MAVS by RIG-I has been shown to depend upon the ubiquitination of RIG-I by the ubiquitin ligase TRIM25 [3], we assayed the effect of TRIM25 in Huh7.25/CD81 cells. Ectopic expression of TRIM25 in Huh7.25/CD81 cells had no effect alone, but resulted in a strong induction of IFN when the cells were infected with Sendai virus, indicating that these cells present a defect in the RIG-I/MAVS pathway at the level of TRIM25. Whatever the nature of this

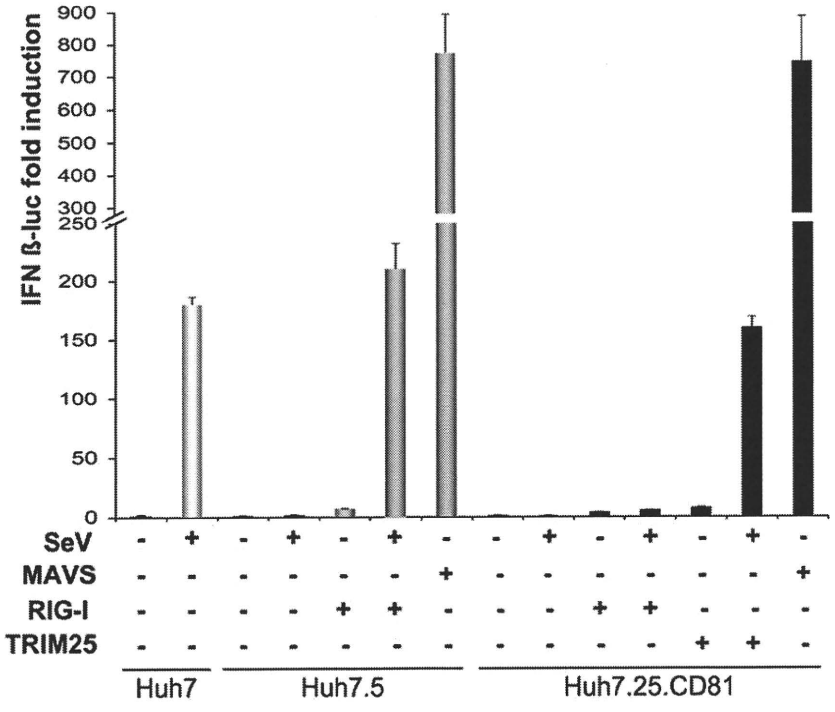

Figure 1. Ectopic expression of TRIM25 restores IFN induction in Huh7.25.CD81 cells. Huh7, Huh7.5 and Huh7.25.CD81 cells were transfected with the pGL2-IFNβ-FLUC/pRL-TK-RLUC reporter plasmids alone or the in presence of plasmids expressing RIG-I (200 ng), TRIM25 (100 ng) or MAVS (400 ng). 24 hrs post transfection, cells were mock-infected or infected with Sendaï virus (SeV) (40 HAU/ml). 24 hrs after infection, luciferase activity was measured and F-luc was normalized against R-luc. IFN expression was expressed as fold induction over control cells that were simply transfected with pGL2-IFNβ-FLUC/pRL-TK-RLUC. Error bars represent the mean ± S.D. for triplicates.
doi:10.1371/journal.pone.0010575.g001

defect, ectopic expression of TRIM25 now allows the use of Huh7.25/CD81 cells as a model to examine the effect of HCV infection on the IFN induction pathway.

HCV specifically stimulates the IFN induction pathway during the first 12 hrs of infection, but inhibits it thereafter

To estimate the time-frame required to study IFN induction before its abrogation upon the action of NS3/4A, we first established the kinetics of MAVS cleavage in the two HCV permissive cell lines Huh7.25/CD81 and Huh7.5 following HCV infection. MAVS cleavage can be detected by immunoblotting, which shows a progressive diminution of the MAVS full-length protein (540 aa) and the apparition of a MAVS cleavage product (513 aa) [2]. In our experimental conditions, MAVS cleavage was clearly detected in both cell types at 48 hrs after infection with JFH1 (Figures 2A and B). Since ectopic expression of TRIM25 in Huh7.25/CD81 cells will be needed in our subsequent experiments designed to examine the effects of HCV on the IFN induction pathway, we also established the kinetics of MAVS cleavage in these cells after their transfection with a plasmid that expresses HA-TRIM25. Under these conditions, MAVS cleavage was clearly observed at 48 hrs (Figure 2C). In all cases, the viral NS3 protease was detected as early as 18–24 hrs, and thereafter its expression increased strongly with time, concomitantly with MAVS cleavage.

Huh7.25/CD81 or Huh7.5 cells were transfected with an IFNβ-luciferase reporter plasmid in the presence of limited amounts of TRIM25 or RIG-I, respectively, and infected with HCV at an moi of 0.2 or with Sendai virus as control. In case of HCV infection, analysis of luciferase activity or of the expression of endogenous IFNβ RNA and HCV RNA was performed in parallel. The results show an increase in luciferase activity that corresponds to an increase in the activation of the RIG/MAVS pathway (Figure 3A,C bottom). This increase was detected as early as 6 hrs after infection for Huh7.25/CD81 cells and 10.5 hrs for Huh7.5 cells, with a maximum expression at 12 hrs for both cell types. The data of the reporter assay were also confirmed at the endogenous level when induction of endogenous IFNβ RNA was assessed by RTqPCR (Figure 3B,D). In both cases, the expression

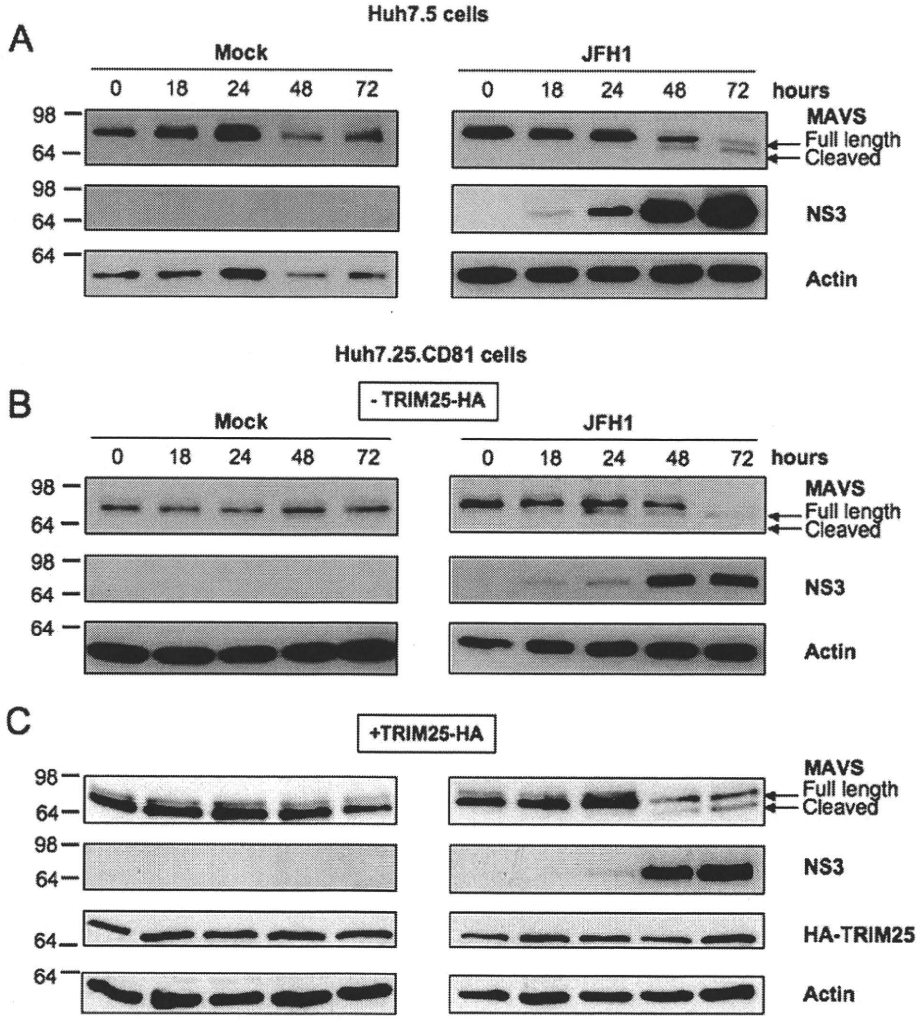

Figure 2. Kinetics of MAVS cleavage in Huh7.25.CD81 cells after JFH1 infection. Huh7.5 cells and Huh7.25.CD81 cells were transfected with an HA-TRIM25 expressing plasmid or with an empty plasmid. 24 hrs post-transfection, cells were mock-infected or infected with JFH1 (m.o.i = 0.05) for the indicated times and cell lysates were generated. Cell extracts (50 μg) were subjected to SDS-12.5% PAGE and blotted with anti-MAVS, anti-NS3, anti-HA or anti-actin as indicated. The arrows indicate the position of full-length MAVS and MAVS cleaved in the presence of HCV NS3/4A.
doi:10.1371/journal.pone.0010575.g002

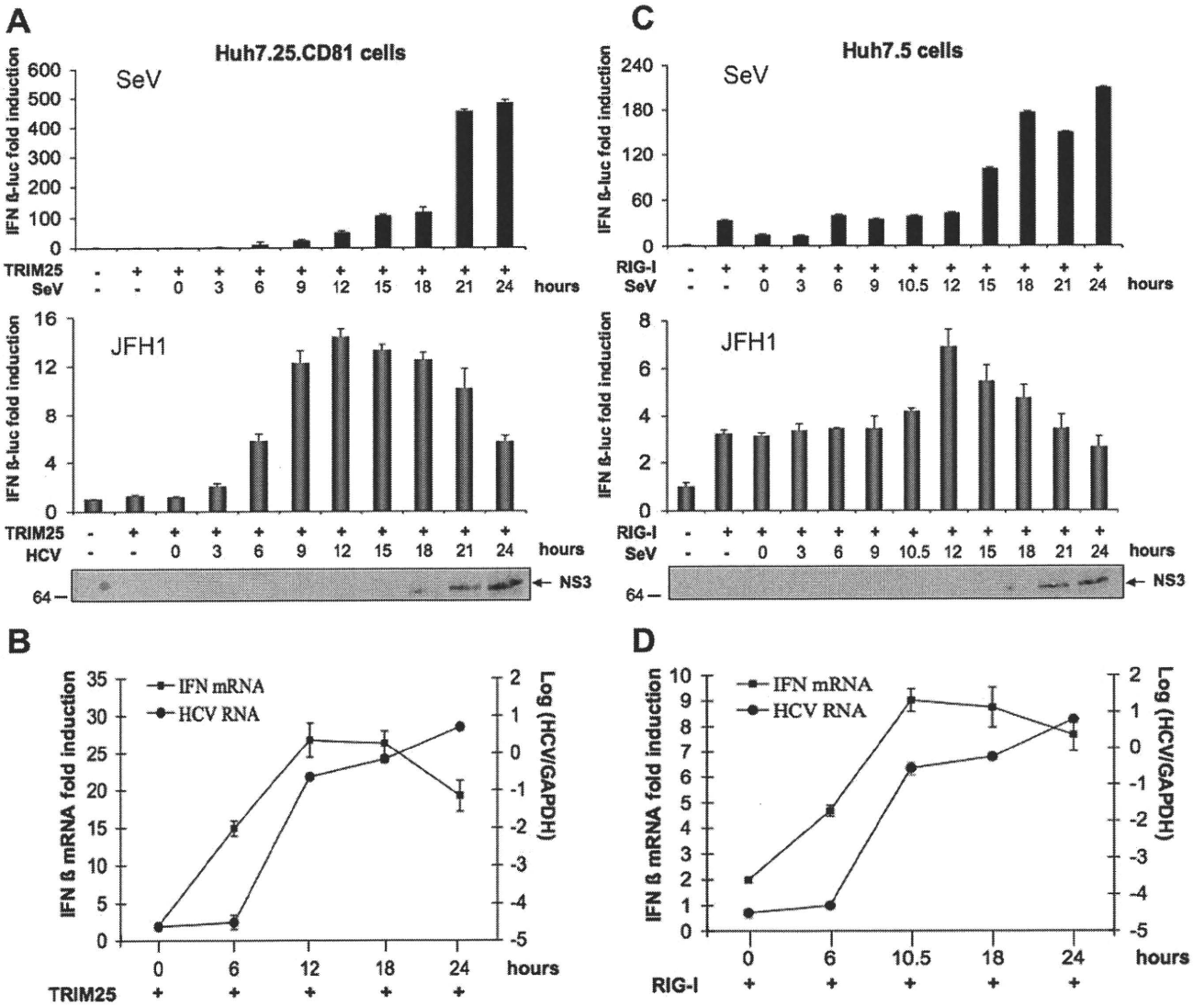

Figure 3. HCV induces IFN during the first 12 hrs of infection and inhibits it thereafter. Huh7.25.CD81 and Huh7.5 cells were transfected with the pGL2-IFNβ-FLUC/pRL-TK-RLUC reporter plasmids together with plasmids expressing HA-TRIM25 (Huh7.25.CD81; A and B) or RIG-I (Huh7.5; C and D). 24 h post-transfection, the cells were infected with SeV (40 HAU/ml) or JFH1 (m.o.i = 0.2). **A and C**: 24 hrs post-transfection, the cells were infected with SeV (40 HAU/ml) or JFH1 (m.o.i = 0.2). At the times indicated, cell lysates were prepared and analysed for IFN induction as described in Materials and Methods. The graphs represent the levels of F-luc activity normalized to R-luc RNA expressed as IFN-β fold-induction over control cells that were simply transfected with pGL2-IFNβ-FLUC/pRL-TK-RLUC. Error bars represent the mean ± S.D. for triplicates. In addition, cell lysates from JFH1-infected cells were pooled and analysed for the presence of NS3 as a marker of HCV infection. **B and D**: 24 hrs post-transfection, Huh7.25.CD81 and Huh7.5 cells were infected with JFH1 (m.o.i = 0.2). At the times indicated, cells were processed for RNA extraction and HCV or IFNβ RNA were quantified by qRT-PCR respectively, and normalized against RNA from GAPDH. Error bars represent the mean ± S.D. for triplicates.
doi:10.1371/journal.pone.0010575.g003

of the viral HCV RNA increases from 6 hrs after infection and continues to rise thereafter. These results indicate that HCV can activate the RIG-I signalling pathway with concomitant IFN induction within the first 12 hrs of infection.

Intriguingly, we observed that after 12 hrs of infection, there was a considerable decline of luciferase activity in both cell types, whereas the levels of endogenous IFNβ RNA remained at a plateau level until 18 hrs, before decreasing at 24 hrs post-infection. The decrease in luciferase expression between 12 and 18 hrs was surprising since NS3 was not fully expressed within this period of time (Figure 3A,C). In contrast, a decrease in luciferase expression at 24 hrs was expected, due to the massive proteolytic cleavage of MAVS by the HCV NS3/4A protease (Figure 2). Inhibition of luciferase activity was shown to be specific to HCV, as infection of both cell types with Sendai virus resulted in a continuous increase of luciferase activity from the IFNβ-luc reporter plasmid (Figure 3A,C top). Altogether, our data indicate that HCV can activate the IFN induction pathway within 12 hrs after infection, but blocks it prior to the NS3/4A-mediated cleavage of MAVS.

HCV activates the phosphorylation of PKR and of its substrate eIF2α, as of 12 hrs post-infection

The results shown in Figure 3 suggested a control of IFN expression by HCV at the protein level. In addition to this, an analysis of the effect of infection on the activity of a different luciferase reporter construct (TK-Renilla luciferase; Figure S1)

revealed a similar specific inhibition at 12 hrs post-infection with HCV and not with Sendaï virus, indicating that HCV could exert a control on protein expression at the general translational level. One possible candidate that could exert such a control is the protein kinase PKR, which inhibits protein synthesis through phosphorylation of the initiation factor eIF2α [13]. Activation of the catalytic domain of PKR is mediated by a change in its conformation due to the interaction of its N terminus with dsRNA structures or with specific proteins [10]. The fact that IFN could be induced during the first 12 hrs post-infection with JFH1 in Huh7.25.CD81/TRIM25 or in Huh7.5/RIG-I cells was an indication that HCV dsRNA structures had appeared in the cytosol that activate RIG-I and that these structures may also represent good candidates to activate PKR. We therefore examined the state and dynamics of phosphorylation of PKR and of its substrate eIF2α upon HCV infection, using Huh7.25/CD81 cells, either as such or upon ectopic expression of TRIM25. At different times post-infection, cell extracts were immunoprecipitated with antibodies directed against PKR or eIF2α, after which the degree of PKR or eIF2α phosphorylation was examined using anti-phospho PKR (residue Thr451) or anti-phospho eIF2α (residue Ser51) antibodies and by performing quantification of the p-PKR/PKR or the p-eIF2α/eIF2α ratio. The results clearly showed peaks of PKR (Figure 4) and eIF2α (Figure 5) phosphorylation as early as 12 and 15 hrs post-infection, followed by a decrease of phosphorylation until 24 hrs and a second increase until 72 hrs post-infection, the end-point of the experiment. The presence of TRIM25 was not found to significantly affect PKR or eIF2α phosphorylation, except for a less abrupt decline between15 and 24 hrs. Altogether, these results show that PKR and its substrate eIF2α are activated in the early hours of HCV infection.

HCV infection triggers inhibition of protein translation

HCV belongs to the family of viruses with 5′ IRES structures that are translated after direct binding of ribosomes to the RNA in the vicinity of the initiation codon. Interestingly, unlike most viral

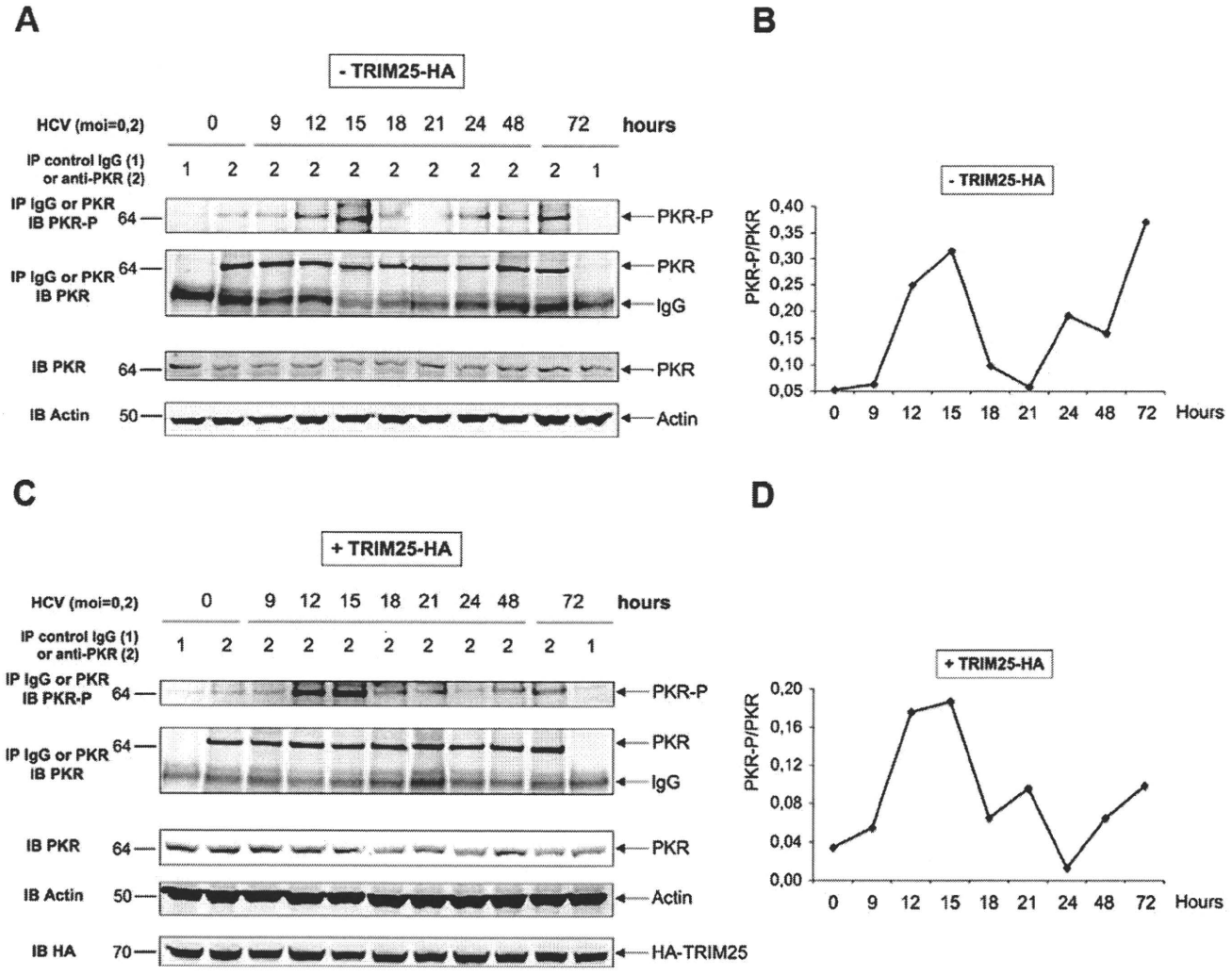

Figure 4. HCV activates the phosphorylation of PKR at 12 and 15 hrs post infection. A and C: Huh7.25.CD81 cells, plated into 100 cm^2 plates, were transfected with the HA-TRIM25 expressing plasmid or with an empty plasmid. 24 hrs post-transfection, cells were infected with JFH1 at an m.o.i of 0.2. At the indicated times post-infection, cell extracts (1 mg) were incubated with Mab 71/10 anti-PKR. In addition, cell extracts prepared at time 0 or at 72 hrs p.i. were incubated with mouse IgG as a control of specificity. The immunoprecipitated complexes were run on two different NuPAGE gels and blotted using Mab 71/10 or anti-phosphorylated PKR (PKR-P). The presence of PKR and PKR-P was revealed using the Odyssey procedure. **B and D**: The bands corresponding to total PKR and their corresponding phosphorylated proteins were quantified using the Odyssey software and expressed as the ratio PKR-P/PKR in the absence (B) or presence (D) of HA-TRIM25.
doi:10.1371/journal.pone.0010575.g004

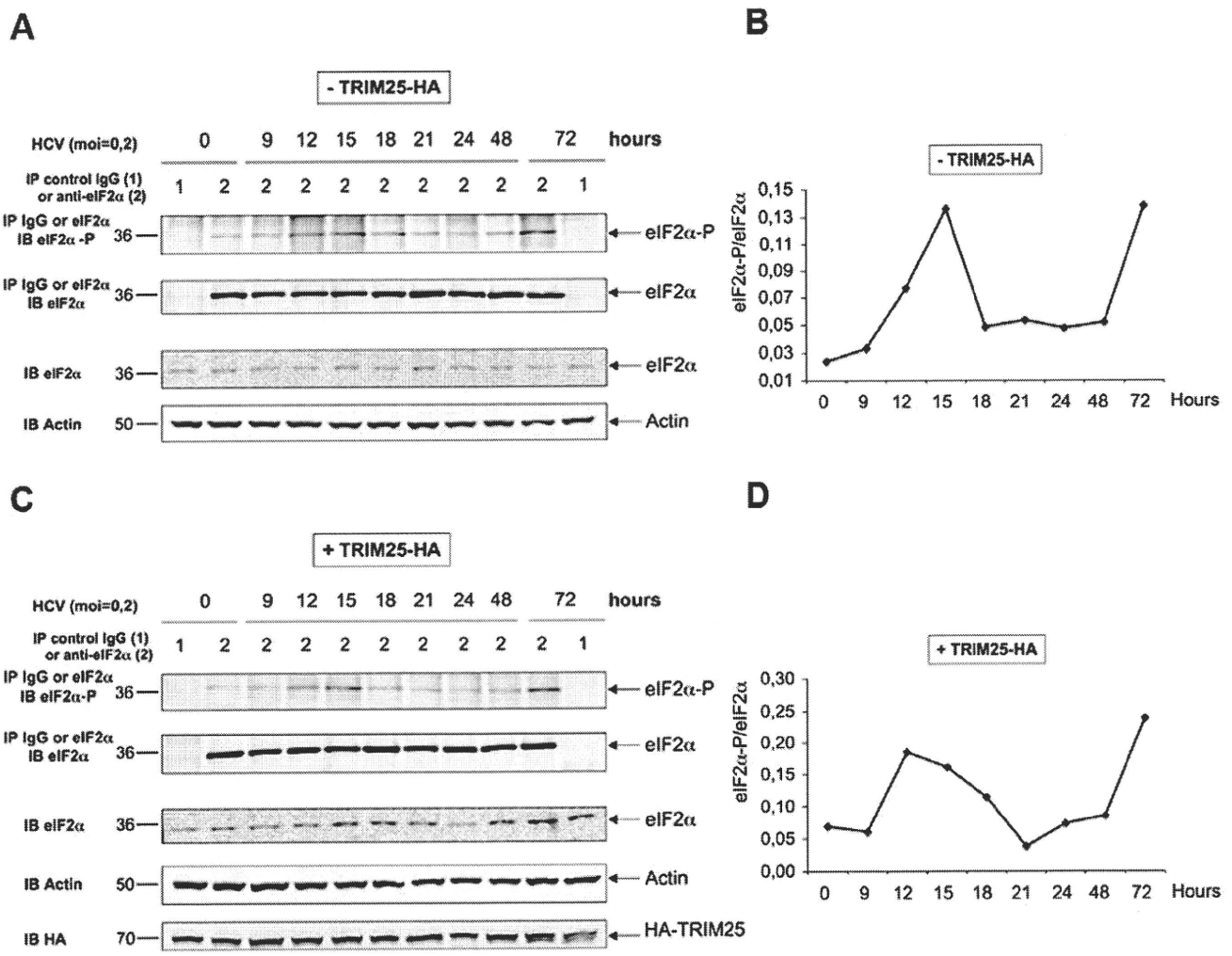

Figure 5. HCV activates the phosphorylation of eIF2α at 12 and 15 hrs post infection. The detection of eIF2α and eIF2α-P and the quantification of the ratio eIF2α-P/eIF2α in the absence (**A and B**) or in the presence (**C and D**) of HA-TRIM25 was performed as described in the legend to Figure 4.
doi:10.1371/journal.pone.0010575.g005

IRESs, translation from the HCV IRES was shown to be independent of eIF2α phosphorylation in situations of stress [14,15]. To establish a correlation between the observed HCV-mediated PKR and eIF2α phosphorylation, and a possible inhibition of eIF2α-dependent translation by HCV, we next compared the effects of HCV infection on the kinetics of expression of a luciferase reporter placed under the control of the IRES^{HCV} (insensitive to eIF2α phosphorylation) or under that of the IRES ^{EMCV} (sensitive to eIF2α phosphorylation). The experiment was done in Huh7.25/CD81 cells transfected with a TRIM25-expressing plasmid, to perform the analysis in conditions leading to IFN induction. For each IRES-luc expressing plasmid, we took care to choose concentrations of these plasmids that give similar levels of RNA expression or luciferase activity (data not shown and Figure 6). After transfection by the different plasmids, the cells were infected with JFH1 and the levels of RNA or luciferase expression followed over 24 hrs. The expression levels of IRES ^{EMCV} RNA and IRES ^{HCV} RNA were found to increase similarly with time post-infection (Figures 6A and C). In contrast, there was a dramatic difference in the expression levels of luciferase expressed from the IRES ^{EMCV} compared to that expressed from the IRES ^{HCV} (Figures 6B and D). Expression of luciferase from the IRES ^{EMCV} was strongly inhibited at 12 hrs post-infection with JFH1, after which time it was progressively restored until at 24 hrs post-infection it approached its initial level. In contrast, expression of luciferase from the HCV IRES was not inhibited at any time after infection with JFH1. Rather, it steadily increased with time post-infection. Similarly to the experiment presented in Figure 3, concomitant analysis of luciferase activity placed under a TK promoter revealed inhibition at 12 hrs post-infection with HCV, regardless of the presence of IRES ^{EMCV} or IRES ^{HCV}, again indicating that the inhibition effect is due to HCV infection and occurs at a general level (Figure S2). These results demonstrate that HCV infection triggers inhibition of general translation, while translation from the IRES ^{HCV} is unaffected. Since inhibition of translation occurs at 12 hrs post-infection, at a time when PKR and eIF2α are phosphorylated (Figures 4 and 5), this shows a correlation between an HCV-mediated inhibition of protein synthesis and PKR/eIF2α phosphorylation; a hallmark of eIF2α-dependent translation.

Depletion of PKR increases IFN induction

We next examined further the role of the ability of HCV to activate PKR in the early events of infection, in relation to IFN

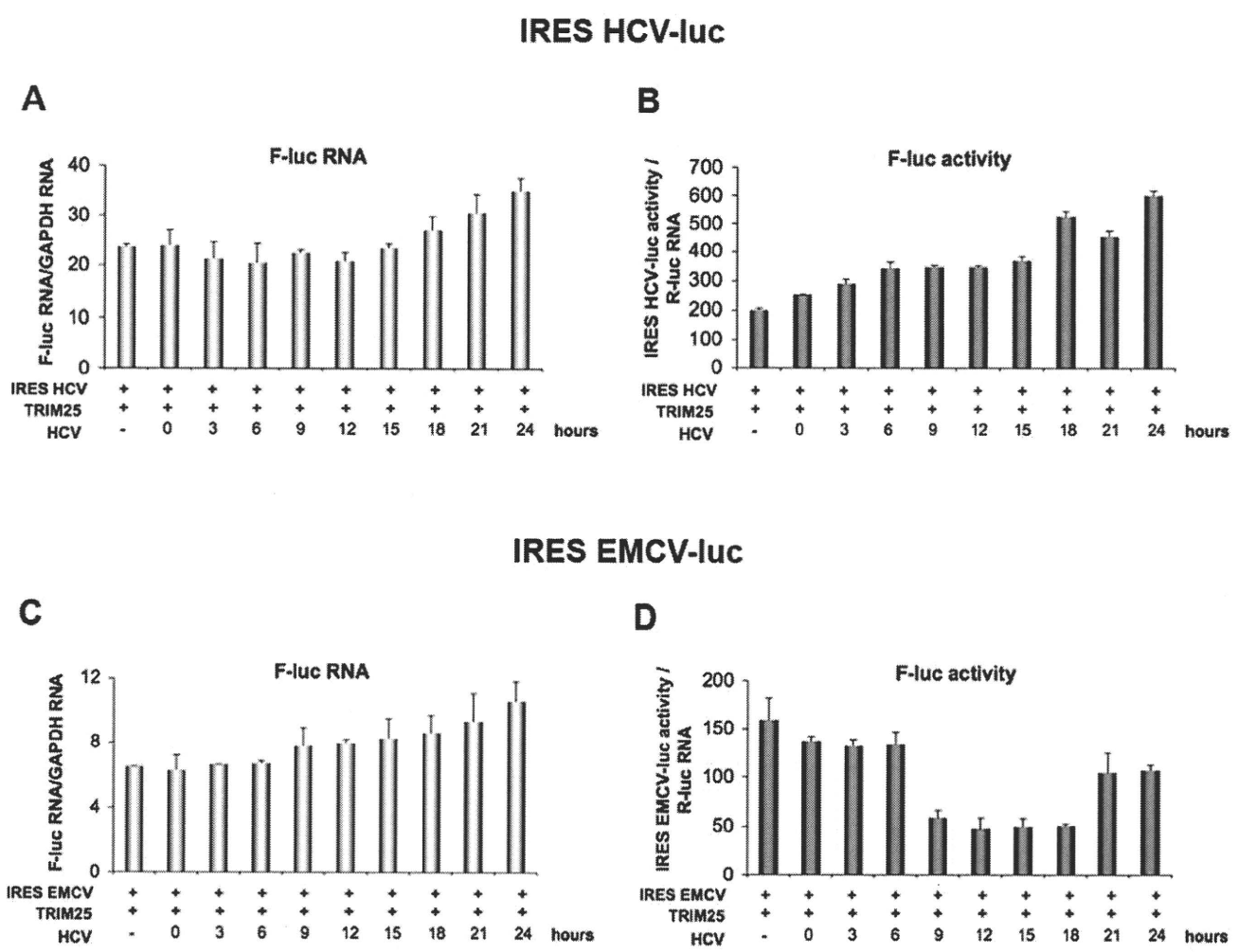

Figure 6. HCV triggers a transient inhibition of protein translation. Huh7.25.CD81 cells were transfected with 400 ng of CAT-IRES^{HCV}-LUC (**A and B**) or 50 ng of CAT-IRES^{EMCV}-LUC (**C and D**), together with the pRL-TK-RLUC plasmid (40 ng) and the HA-TRIM25 expressing plasmid (100 ng). 24 hrs post-transfection, cells were infected with JFH1 at an m.o.i of 0.2. **A and C**: At the indicated times, total cellular RNA was extracted and F-luc and GAPDH RNA were quantified by qRT-PCR. The graphs represent the number of copies of the IRES^{HCV}-luc (A) or of the IRES^{EMCV}-luc (C) RNA normalized to the number of copies of GAPDH RNA. Error bars represent the mean ± S.D. for triplicates. **B and D**: At the indicated times, cell lysates were prepared and the IRES^{HCV}-luc or IRES^{EMCV}-luc activity was analysed by a reporter assay. For normalization, the levels of firefly luciferase activity were divided in each case by the ratio R-luc RNA/GAPDH RNA that was calculated after measurement of the R-luc RNA by RTqPCR using the total cellular RNA extracted for A and C. Error bars represent the mean ± S.D. for triplicates.
doi:10.1371/journal.pone.0010575.g006

induction. Huh7.25/CD81 cells were transfected with control siRNAs or siRNA directed against PKR, in conditions that allow complete depletion of PKR (Figure 7B). They were then transfected with TRIM25 in the presence of the IFNβ-luciferase reporter plasmid. Cells that express normal endogenous levels of PKR presented an initial increase in IFNβ-luciferase induction up to 12–15 hrs in response to infection with JFH1 followed by a sudden decline (Figure 7A), similarly to the results described in Figure 3. In contrast, induction of IFNβ-luciferase continued to increase past 15 hrs post-infection in cells in which PKR expression was silenced. In both cases, a decrease of IFN expression at 24 hrs was correlated with strong NS3 expression in the cytosol (Figure 7A). Concomitant analysis of the activity of luciferase placed under a TK promoter revealed the same pattern of inhibition of expression during HCV infection, which was alleviated when PKR was silenced. This confirmed that HCV-mediated inhibition at the general level occurs through PKR (Figure S3). Therefore, these results demonstrate the role of PKR activation in controlling IFN induction in HCV infection prior to MAVS cleavage by the HCV NS3/4A.

PKR positively controls HCV yields through the inhibition of the IFN induction pathway

We next examined whether there was a correlation between the control of IFN induction by PKR, and HCV yields. Huh7.25/CD81 cells were transfected with control siRNA or siRNA directed against PKR as in Figure 7, and infected with JFH1, in conditions where the IFN induction pathway was either active after transfection with TRIM25, or not (Figure 8). The virus yields were measured by RT-qPCR at different times post-infection. First, ectopic expression of TRIM25 triggered a significant inhibition of virus yields at 24 hrs post-infection (40%; Figure 8), as expected from its ability to restore IFN induction in Huh7.25/CD81 cells as shown in previous figures. Inhibition of virus yields

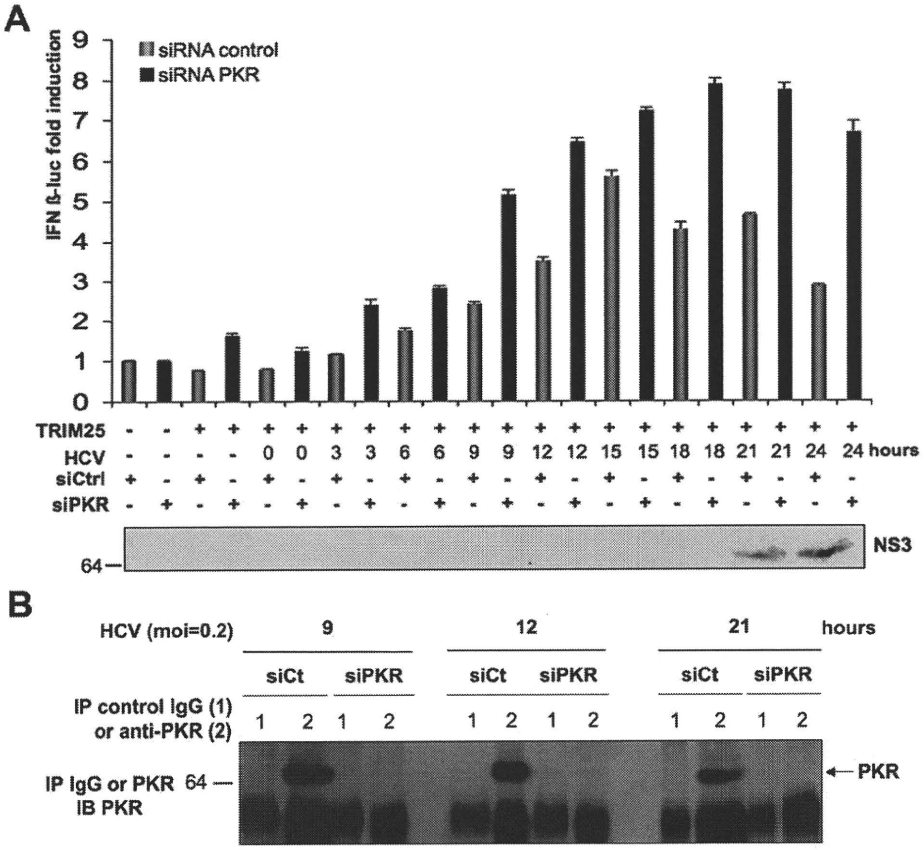

Figure 7. Depletion of PKR increases IFN induction in HCV-infected cells. Huh7.25.CD81 cells were first transfected with 25 nM of siRNA directed against PKR or with 25 nM of control siRNA and then transfected 24 hrs later with the pGL2-IFNβ-FLUC/pRL-TK-RLUC reporter plasmids and the TRIM25 expressing plasmid. 24 hrs post-transfection the cells were infected with JFH1 at an m.o.i. of 0.2. **A**: At the indicated times, one set of cells was treated for RNA extraction and the other for reporter assay as described in the legend to Figure 3. IFN expression was expressed as fold-induction over control cells that were simply transfected with pGL2-IFNβ-FLUC/pRL-TK-RLUC and either control siRNA or siPKR. The graph represents the levels of firefly luciferase activity normalized to the ratio R-luc RNA/GAPDH RNA. Error bars represent the mean ± S.D. for triplicates. In addition, cell lysates were pooled and analysed for the presence of NS3 as a marker of HCV infection. **B**: Huh7.25.CD81 cells were treated as in A, except for transfection with the reporter plasmids, to control the efficiency of PKR silencing. At the indicated times post-infection, cell extracts (1.7 mg) were incubated with normal mouse IgG or Mab 71/10 anti-PKR. The immunoprecipitated complexes were run on SDS-12.5% PAGE gels and blotted using Mab 71/10 (PKR).
doi:10.1371/journal.pone.0010575.g007

did not increase later in infection (36% at 48 hrs post-infection; Figure 8), in agreement with the block on IFN induction downstream of TRIM25 imposed by the NS3/4A-mediated cleavage of MAVS. Depletion of PKR from Huh7.25/CD81 cells also triggered inhibition of virus yields. Interestingly, whereas this inhibition was limited in the absence of TRIM25 (13% and 9% inhibition at 24 and 48 hrs post-infection, respectively), it was more pronounced when the cells were expressing TRIM25, with a 28% and 31% further increase in inhibition after 24 and 48 hrs of infection, respectively (Figure 8). Altogether, the combined effect of TRIM25 expression and PKR depletion resulted in 58% of inhibition of HCV virus yields at 24 hrs and 56% at 48 hrs post-infection. These data demonstrate that HCV infection is particularly sensitive to the IFN induction pathway, and that the efficiency of infection benefits from an inhibition of this pathway at the translational level by PKR.

Pharmacological inhibitors of PKR increase IFN induction and inhibit HCV infection

Although best known for its antiviral proprieties, PKR is now also recognized for its negative effect on neurodegenerative disorders such as Huntington's, Parkinson's and Alzheimer's diseases [16]. For these reasons, pharmacological inhibitors of PKR have been developed. Here, we have used two PKR inhibitors, the oxindole-imidazole C16 compound [17] and the cell penetrating PRI peptide, that corresponds to one PKR motif (DRBM) involved in binding to its activators. This latter compound represents a more specific PKR inhibitor than C16 [18]. We examined the effects of these inhibitors on IFN induction and HCV replication during infection of Huh7.25/CD81 cells with JFH1 (Figure 9). The cells were transfected with TRIM25 as described in Figure 7, and incubated with either C16 or PRI after 11 hrs of infection. The results clearly show that both PKR inhibitors increased IFNβ promoter induction (Figure 9A), as well as restoring general level of protein expression (Figure S4). This increase was more pronounced at 15–18 hrs post-infection (Figure 9A). This highlights the importance of PKR activation during this time-frame to control IFN induction. Next, the effect of the PKR inhibitors on HCV replication was assayed. Huh7.25/CD81 cells were transfected with TRIM25, or not, to have a non-functional or functional RIG-I/MAVS pathway. Similarly to the experiment shown in Figure 8, PKR inhibitors were able to inhibit HCV yields only in conditions where the RIG-I/MAVS pathway was activated (Figure 9B).

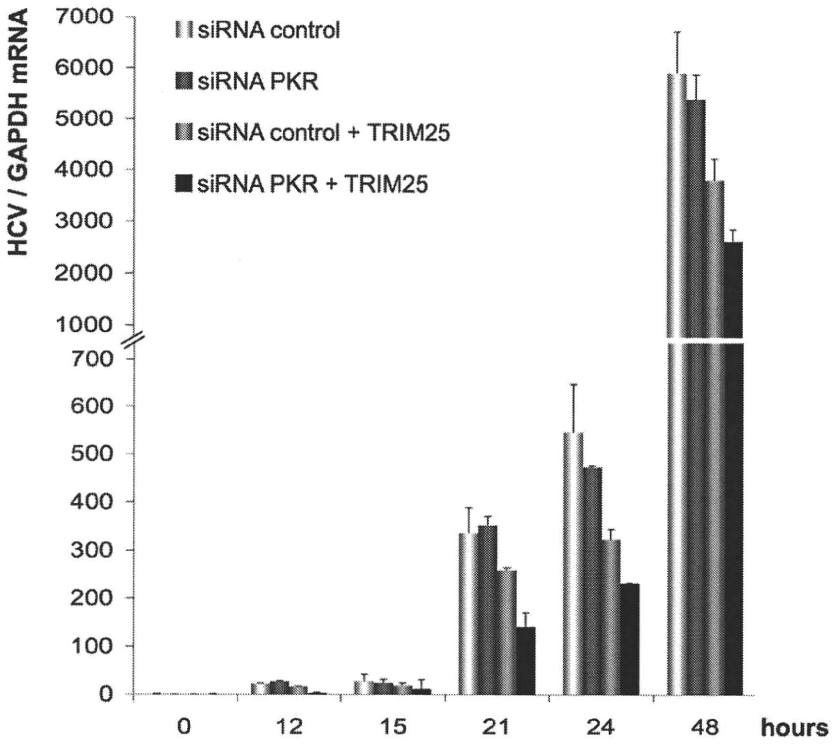

Figure 8. PKR positively controls HCV yield through inhibition of the IFN induction pathway. Huh7.25.CD81 cells were first transfected with 25 nM of siRNA directed against PKR or 25 nM of control siRNA and then transfected 24 hrs later with either empty vector or the TRIM25 expressing plasmid. 24 hrs post-transfection, the cells were infected with JFH1 at an m.o.i. of 0.2. At the indicated times, cells were processed for RNA extraction and HCV RNAs were quantified by qRT-PCR and normalized against RNA from GAPDH. Error bars represent the mean ± S.D. for triplicates.
doi:10.1371/journal.pone.0010575.g008

Discussion

Here we report the use of HCV permissive Huh7.25.CD81 cells to analyse the effect of HCV on the RIG-I/MAVS-mediated IFN induction pathway during the early hours after infection, before the HCV NS3/4A protease can cleave MAVS and abrogate this pathway. We first observed that the IFN induction pathway was deficient in these cells, but that it could be conveniently restored upon ectopic expression of the E3 ubiquitin ligase TRIM25. This protein has been shown to bind the threonine 55 residue of RIG-I through its C terminal SPRY domain, and uses the E3 ligase activity present in its N terminal RING domain to promote a Lys63-type ubiquitination of RIG-I in its CARD domain at lysine 172. This modification is important if RIG-I is to engage in a correct interaction with its downstream adapter MAVS [3]. The nature of the TRIM25 defect in Huh7.25.CD81 cells and the relation to activation of RIG-I is now under characterization. It is interesting to note here that this defect emphasizes the importance of the RIG-I/TRIM25 pathway in the control of HCV expression since both Huh7.25.CD81 and Huh7.5 cells, which were originally selected for their ability to replicate HCV subgenomic replicons, present a defect in this pathway at the level of RIG-I for Huh7.5 cells and of TRIM25 for Huh7.25.CD81 cells. Importantly, Huh7.25.CD81 cells can be considered as a more physiological model than Huh7.5 cells to study the interaction between the IFN induction pathway and HCV infection, since Huh7.5 cells have a point mutation at the threonine 55 residue of RIG-I [5] and therefore require ectopic expression of RIG-I to restore their IFN induction pathway. In contrast, ectopic expression of TRIM25 restores the IFN induction pathway downstream of RIG-I and therefore does not perturb the initial interaction between RIG-I and the incoming HCV dsRNA structures.

Using Huh7.25.CD81 cells that ectopically express TRIM25, we observed that HCV triggers IFNβ induction as early as 6 hrs after infection, demonstrating that the entry of the virus into the cell rapidly generates enough viral structured RNAs to activate RIG-I. NS3/4A expression was detected around 18 hrs post-infection, and MAVS cleavage after 24 hrs post-infection. We thus expected to observe an increase in IFNβ induction at least until 18 hrs after infection. This was indeed found to be the case when we analysed IFNβ induction at the RNA level. However, when we used a luciferase reporter gene placed under the IFNβ promoter as a surrogate marker for production of the IFNβ protein, it was intriguing to observe an arrest of IFN induction as rapidly as 12 hrs after infection, followed by a considerable decline in its expression afterwards. These results indicated a new control of IFN induction at the translational level during HCV infection in addition to –and earlier than- the NS3/4A-mediated MAVS cleavage. We have demonstrated that this inhibition is the result of a strong activation of the protein kinase dsRNA-dependent kinase PKR at 12 and 15 hrs after HCV infection and of the concomitant phosphorylation of its substrate eIF2α.

Since this manuscript was submitted, work performed by U.Garaigorta & F. Chisari showed that HCV also activates PKR and eIF2α phosphorylation to negatively control the antiviral action of IFN[19]. Both their and our data concur to point out that HCV diverts PKR away from its known antiviral role to use it to attenuate both the IFN-mediated antiviral response [19] and IFN induction itself (our data). Importantly, both studies show that PKR silencing has no effect on HCV production, unless cells are

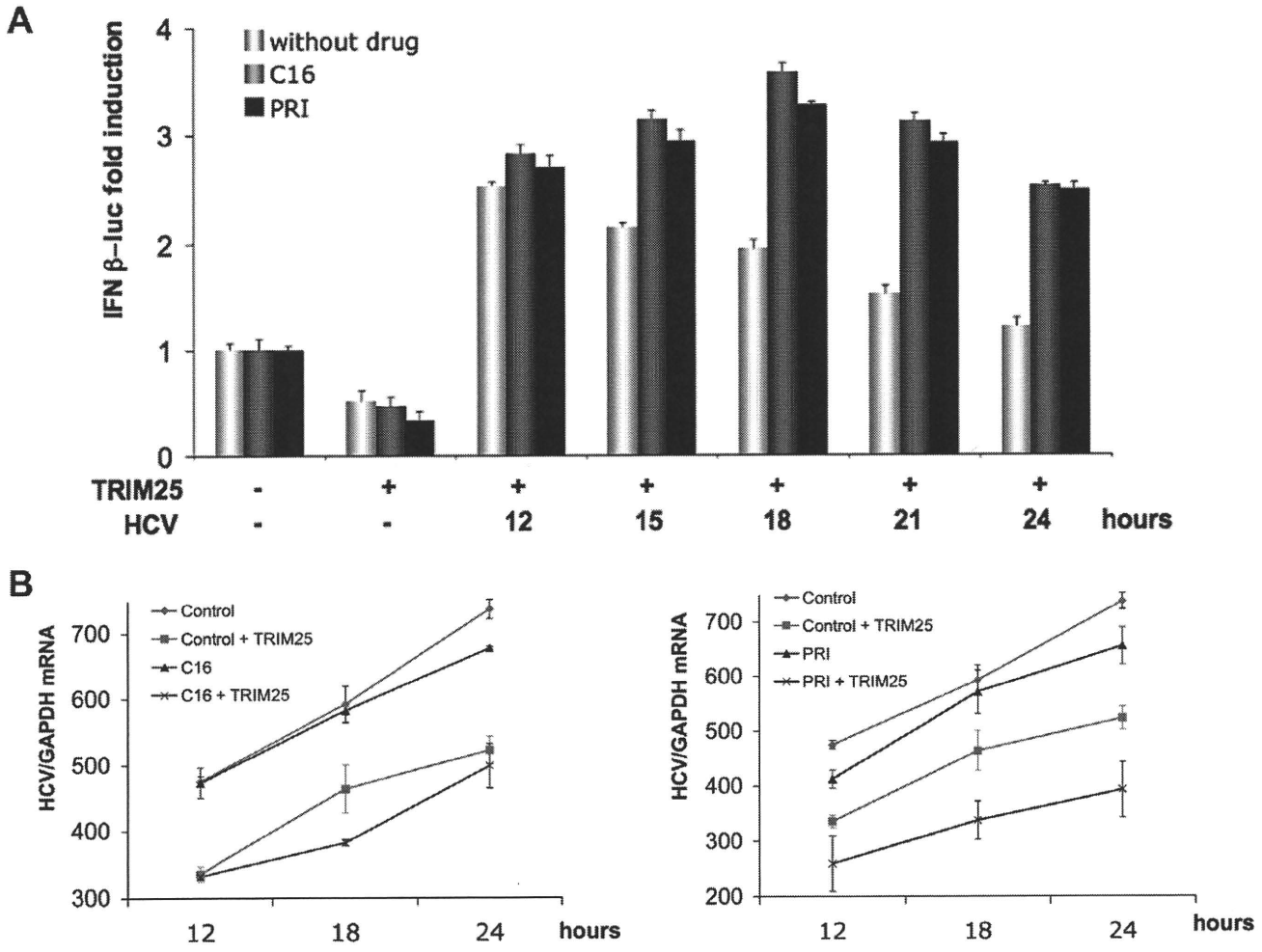

Figure 9. Pharmacological inhibitors of PKR increase IFN induction and inhibit HCV infection. A: Huh7.25.CD81 cells were first transfected with the pGL2-IFNβ-FLUC/pRL-TK-RLUC reporter plasmids and the TRIM25 expressing plasmid. 24 hrs post-transfection, the cells were infected with JFH1 at an m.o.i of 0.2. At 11 hrs post-infection, cells were exposed to 200 μM of C16 or 30 μM of the PRI peptide as described in Materials and Methods. At the indicated times, one set of cells was treated for RNA extraction and the other for reporter assay as described in the legend to Figure 3. IFN expression was expressed as fold-induction over control cells that were simply transfected with pGL2-IFNβ-FLUC/pRL-TK-RLUC. The graph represents the level of firefly luciferase activity normalized to the ratio R-luc RNA/GAPDH RNA. Error bars represent the mean +/- S.D. for triplicates. **B**: Huh7.25.CD81 cells were first transfected with the TRIM25 expressing plasmid or an empty plasmid. 24 hrs post-transfection, the cells were infected with JFH1 at an m.o.i of 0.2. At 11 hrs post-infection, cells were exposed to 200 μM of C16 or 30 μM of the PRI peptide as described in Materials and Methods. At the indicated times, cell lysates were processed for RNA extraction and HCV RNAs were quantified by qRT-PCR and normalized against RNA from GAPDH. Error bars represent the mean +/- S.D. for duplicates.
doi:10.1371/journal.pone.0010575.g009

allowed to induce IFN upon ectopic expression of TRIM25 (our study) or are directly treated with IFN [19].

PKR is a 551 aa serine/threonine protein kinase with its catalytic domain at the C-terminus and regulating domains at the N-terminus. This N-terminus domain contains two tandem copies of a 70-amino acid dsRNA binding motif or DRBM (positions 6–79 and 96–169) that affiliate PKR to the large family of dsRNA binding proteins, which includes TRBP, PACT, DICER, ADAR, RNAse III and NFAR's [20]. Binding of PKR to dsRNA induces its dimerization and a change of its conformation that frees access to its autophosphorylation site. Structural analysis has revealed that PKR dimers are arranged back to back, which prevents trans-phosphorylation of one monomer by the other and favours a model of autophosphorylation in cis or through the action of a PKR dimer on other PKR dimers or monomers [21]. Once autophosphorylated on its threonine T446, PKR is stabilized as a kinase and can phosphorylate its substrates, such as the α subunit of the initiation factor eIF2. PKR is preferentially activated upon binding to long stretches of dsRNA (>33 bp) [22] but was recently shown also to be activated upon binding to RNA structures similar to those that activate RIG-I, such as short imperfect 16 bp stem-loop RNAs with 5′ triphosphorylated ends. It is now proposed that perfect dsRNAs can activate PKR with no need for a 5′ppp, whereas if they are to activate, dsRNA with minimal secondary structures are dependent on 5′ppp [23]. In addition, PKR activity can be regulated positively and negatively through interaction with the cellular proteins PACT and TRBP, two members of the dsRNA binding protein family. This type of interaction, which is independent of the presence of dsRNA, is complex. The TRBP/PACT interaction can modulate the activation of PKR by PACT and a cellular stress reverses it [24].

Our results point out the ability of HCV to trigger both induction of IFN and activation of PKR in the early hours of infection. The induction of IFN is initiated by the binding of RIG-

I to viral 5′ppp structured RNA, the 3′ end poly-U/UC motif and/or replicative RNA duplexes [5,25]. In vitro experiments have shown that PKR can be activated upon binding to the HCV IRES [26] but it is currently not known exactly how HCV activates PKR in vivo. The use of antibodies directed against phosphorylated PKR or against phosphorylated eIF2α allowed in vivo activation of PKR to be demonstrated, either upon HCV subgenomic replicon replication [27] or more recently after electroporation of Huh7 cells with JFH1 RNA [28]. Surprisingly, the latter study showed that silencing of PKR resulted in 10-fold higher viral yields compared to our study (Figures 8 and 9) and that of Garaigorta & Chisari [19], where no effect on viral yields could be observed unless the IFN induction pathway is triggered or IFN is added to the cells. Although it is difficult to compare different experimental systems, the discrepancy observed may be due to the different procedures used to express JFH1 in the cells: electroporation of its RNA in Kang'study, compared to infection with JFH1 viral stocks in our study and that of Garaigorta & Chisari. Interestingly, the differences might indicate that the mode and/or efficiency of interaction between the HCV structures required to activate PKR are crucial to determine how the virus will benefit or suffer from PKR action. PKR has also been shown to be activated through an interaction between its N terminal domain and the first 58 amino acids of HCV core protein [29]. Core is the first HCV protein to be processed upon translation of the viral polyprotein and may interact with endogenous PKR soon after its own apparition in the cytosol. The possibility evoked here that core is involved in PKR activation requires further investigation.

Our results show that the IFN induction pathway can be stimulated during HCV infection up to 12 hrs post-infection, followed by a decline concomitantly with activation of PKR and of its substrate eIF2α. Importantly, depletion of the endogenous PKR by silencing, or inhibition of its function through the use of pharmacological inhibitors, prevents this decline. This indicates that HCV infection triggers an inhibition of general protein synthesis through PKR, whereas its own translation is not affected, as shown by the appearance of the viral proteins and an increase in expression of a reporter gene placed under the control of an IRES ^{HCV}. These data are in agreement with a recent study which showed, using in vitro experiments, that PKR can inhibit both cap-mediated and IRES ^{EMCV}-mediated translation, but not IRES ^{HCV}-mediated translation [26]. Shimoike et al proposed that HCV uses alternate initiation factors that allow a mechanism of translation initiation distinct from other IRES and from the cellular machinery of general translation that is not inhibited by eIF2α phosphorylation. The resistance of IRES ^{HCV} to control of translation may be related to a positive effect *in trans* from the virus through some of its structures, such as the polyadenylated 3′ UTR [30]. Alternatively, translation from the HCV IRES may occur in autophagy-like structures, together with translation from the incoming HCV RNA, where it may escape PKR action [31]. By both escaping and down regulating host cap-dependent translation, HCV may gain a further selective advantage for its own replication and propagation.

Interestingly, we found that the depletion of PKR from Huh7.25.CD81 cells, or incubation with the PKR inhibitors C16 and PRI, leads to inhibition of HCV replication, but only under conditions where the IFN induction pathway has been restored by the expression of TRIM25. Our results thus demonstrate that, among all the cap-dependent proteins the expression of which are sensitive to PKR, only the translation of proteins resulting from the activation of the IFN induction pathway represent a real constraint for HCV replication and propagation. Early activation of PKR upon HCV infection (12–15 hrs post-infection) allows this virus to limit the expression of IFN and pro-inflammatory cytokines as soon as possible, before enough NS3/4A is translated from the HCV IRES to block this signaling pathway through MAVS cleavage (18 to 24 hrs post-infection) (see model in Figure 10). Through detailed kinetic experiments, we demonstrated that phosphorylation of PKR and of its substrate eIF2α are restricted to a 3 hour-period between 12 and 15 hrs post-infection. Accordingly, the PKR inhibitors C16 and PRI efficiently restored IFN induction during this time. The use of both PKR silencing and the addition of pharmacological inhibitors of PKR demonstrates the importance of PKR in the control of IFN induction early after infection with HCV. These results highlight that the 3-hour period between 12 and 15 hrs post-infection is crucial for HCV to activate PKR to restrain IFN expression, once it has launched the IFN induction pathway through interaction of its replicative dsRNA forms with RIG-I. Its ability to activate PKR at the same time allows this induction to be moderated at the level of the translation of this cytokine before sufficient NS3/4A accumulates and abrogates IFN induction at the transcriptional level through MAVS cleavage.

It was intriguing to observe that PKR and eIF2α phosphorylation decrease at 15 hrs post-infection with HCV, to reappear progressively and increase from 24 hrs post-infection until the 72 hr end-point of the experiment (Figures 4 and 5). The reason for this remains to be investigated and may indicate that PKR could be sensitive to the action of phosphatase(s) at certain time points of the infection.

PKR is well-recognized as an important effector of the antiviral response through its ability to arrest protein synthesis and its importance is highlighted by the number of viral and cellular products that are able to abrogate or modulate its action [13,32]. In the case of HCV, some viral proteins such as NS5A and a cytosolic soluble form of E2 were reported to interact with PKR, and were proposed to be viral inhibitors of the antiviral action of PKR [33,34,35].

Here, we show another aspect of the interaction of HCV with PKR, that reveals how HCV uses the ability of PKR to inhibit cellular cap-dependent translation, while avoiding its effect through its own translation driven by the HCV IRES. PKR silencing or PKR inhibitors have less effect on HCV production when the RIG-I/MAVS pathway is non-operative. This demonstrates that it is only IFN (and presumably also the pro-inflammatory cytokines resulting from the activation of the RIG-I/MAVS pathway) that represents a threat for viral propagation. The situation we describe here might correspond to primo-infection during the natural course of HCV infection in an IFN-free environment, allowing unabated propagation of the virus due to very limited production of IFN. In established chronic infections, whatever IFN has been produced can then trigger induction of a large number of ISGs (IFN-stimulated genes), such as RIG-I and TRIM25, which can sustain the IFN induction pathway, and ISG56 or viperin, which are involved in the inhibition of HCV translation and replication [36,37]. Although PKR is also recognized in several viral infections for its antiviral proprieties, it may be more suitable to control its action in the case of HCV infection. Therefore, we propose that a carefully-controlled use of PKR inhibitors, in conjunction with IFN/ribavirin, would be beneficial for the treatment of chronically HCV-infected patients, since it would lead to a boost in the induction of innate immunity and a sustained inhibition of the viral propagation.

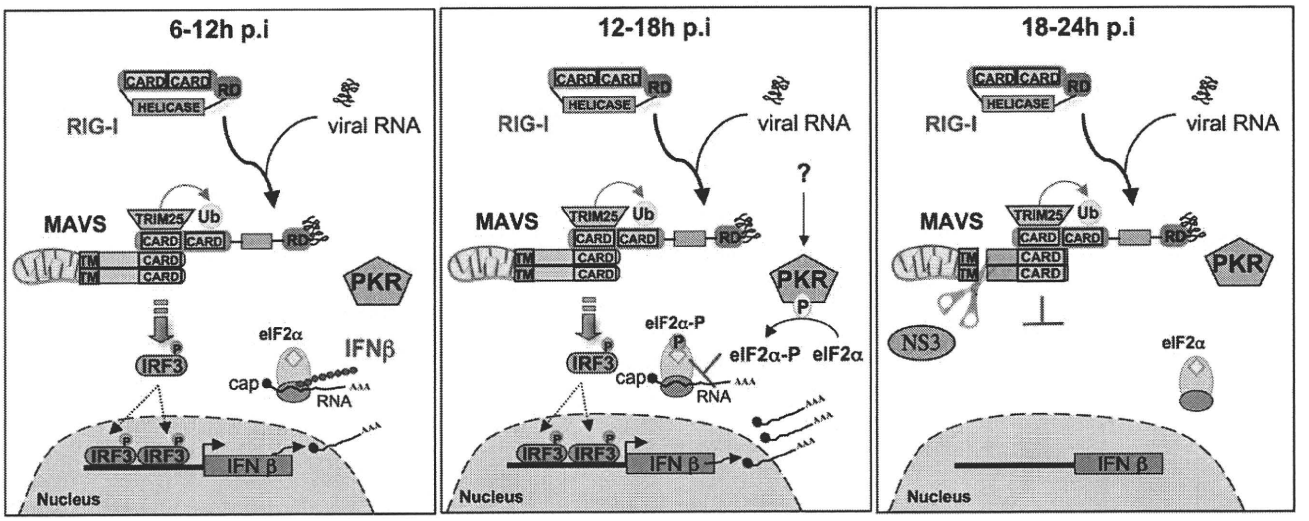

Figure 10. Model of regulation of IFN β induction at the very early steps of HCV infection. Left panel: *6–12 hrs after infection.* After cell entry, the HCV genomic RNA is liberated, and thus dsRNA structures are accessible in the cytosol and can associate with the RIG-I RNA helicase. This triggers activation of RIG-I followed by its ubiquitination by the E3-ligase TRIM25, and interaction with the mitochondria-bound MAVS adapter. MAVS, in turn, activates downstream signalling kinases leading to IRF3 phosphorylation and induction of IFNβ. Detection of IFNβ expression starts at 6 hrs p.i. and increases until 12 hrs post-infection. Induced IFNβ mRNA moves to the cytosol and is translated into IFNβ protein through the cap-dependent process of cellular translation. **Middle panel:** *12–18 hrs after infection.* HCV infection triggers the activation of PKR through a still unknown mechanism (either through its dsRNA or through a viral protein, such as core, or through activation of a cellular protein, such as PACT). Once activated, PKR phosphorylates its substrate, the α subunit of the eIF2 initiation complex and arrests the cap-dependent protein synthesis. As a result, translation of IFNβ protein stops. **Right panel:** *18–24 hrs after infection.* HCV proteins have been translated through a cap-independent mechanism and begin to accumulate in the cytosol. The viral NS3 protease cleaves MAVS at residue 508. This results in complete inactivation of MAVS, arrest in the recruitment of its downstream kinases and arrest of IFN induction. Note that after 15 hrs, PKR is no longer phosphorylated, hence no longer activated. The mechanism of this regulation is not yet known. RIG-I: Retinoic acid Inducible Gene 1; CARD: Caspase Recognition Domain; RD: Repressor Domain, Ub:Ubiquitin; MAVS: Mitochondria Adaptor Virus Signalling; TM: Transmembrane domain; PKR: Protein Kinase RNA-dependent; IRF3: Interferon Regulatory Factor 3; eIF2α: α subunit of eukaryotic Initiation Factor; AAA: polyadenylated tail. P: phosphate group.
doi:10.1371/journal.pone.0010575.g010

Materials and Methods

Cell culture

Huh7 and Huh7.5 cells were cultured in Dulbecco's modified Eagle's Medium (DMEM; Sigma) supplemented with 10% heat-inactivated fetal bovine serum, 1% nonessential amino acids (Gibco BRL) and 1% penicillin/streptomycin (Invitrogen). Huh7.25/CD81 cells were cultured in the same medium supplemented with 0.4 mg/ml geneticin (G418; PAA Laboratories).

Viruses

Sendai virus stocks were grown in the allantoic cavities of 9-day-old embryonated chicken eggs that were provided by D. Garcin, as described [38]. For the preparation of HCV stocks, Huh7.5 cells plated in 150 cm^2 flasks were inoculated with JFH1 at an m.o.i of 0.05, in serum-free DMEM. After 2 hrs at 37°C, the medium was removed and replaced with complete medium. Three days after infection, the cells were dissociated by trypsin treatment, and replated in 3 or 4 150 cm^2 flasks. After 3 more days, the JFH1-containing cell supernatants were collected, centrifuged at 1200 rpm for 10 min at 4°C, cleared of debris by passing through 0.45-µm-pore-size filters, and stored at −80°C. The cells were trypsinated once again, passaged in 1 or 2 150 cm^2 flasks and viral supernatants were collected again after 24 hrs and stored at −80°C. For titration, Huh7.5 cells (10^5 cells/well in a 24-well plate) were incubated in the presence of serial dilutions of the viral preparations. After three days, cells were washed with PBS, fixed for 20 min with 4% paraformaldehyde-PBS (PFA; Electron Microscopy Sciences), permeabilized by incubation for 1 hour with PBS that contained 1% gelatin (Sigma) and 0.1% Tween-20 (Sigma), and incubated for 1 hour with 150 µl of PBS-gelatin that contained serum from a patient chronically infected with HCV (genotype 1b) at a 1/500 dilution. Cells were washed and incubated with peroxidase-conjugated anti-human antibody (1/2500 dilution; Dako), and the presence of the virus was detected using the Vector NovaRED substrate kit for peroxydase (VECTOR). Infectious foci were counted under a microscope and the titer was calculated as focus forming units per ml. Titers of 6.10^4 FFU/mL were obtained on a routine basis.

Plasmids, siRNAs and antibodies

The pcDNA3 expressing 5'HA tagged-TRIM25 was provided by D. Garcin. The CAT-IRES^{HCV}-LUC and CAT-IRES^{EMCV}-LUC constructs have been described [39]. The IFNβ-firefly luciferase (pGL2-IFNβ) and pEF-BOS FLAG-RIG-I plasmids were described previously [40]. The pcDNA3.1 cMyc-MAVS has been described [41]. Control (scrambled) siRNA and siRNA to PKR (GCAGGGAGUAGUACUUAAAUAUU) were synthesized by Dharmacon Research, Inc. (Lafayette, CO). The siRNAs (final concentration 25 nM) were transfected for 24 h using FuGENE HD (ROCHE) before the transfection with other plasmids, or infection. Normal mouse IgG were from Santa Cruz Biotechnology. Monoclonal anti-PKR 71/10 antibody was obtained from A.Hovanessian [42]. Anti-actin antibody was from Sigma. Rabbit polyclonal antibodies were used to detect eIF-2α phosphorylated at Serine 51 (Cell Signalling Technology), PKR phosphorylated at Thr451 (AbCAM), and MAVS (Alexis Biochemical Inc.). Mouse monoclonal antibodies were used to detect HCV NS3 and the HA tag (Chemicon and 12CA5; Roche, respectively).